CODEN:LUTEDX/(TEIE-5468)/1-50/(2021)

Industrial Electrical Engineering and Automation

Torque Ripple Analysis and Compensation of Servo Drives for Robot Application

August Millqvist

Division of Industrial Electrical Engineering and Automation
Faculty of Engineering, Lund University

Contents

1 Introduction

1.1 Background

Permanent Magnet Synchronous Motors (henceforth referred to as PMSM) are commonly used in many applications such as power tools, electric vehicles and robotics [1]. These motors are often implemented in industrial robot servo systems which include a driver and motor, referred to as servo motors and servo drives.

Robotics is a field of use for servo systems with very high expectations on the system's performance. In general, industrial robots are controlled with a cascade control structure. Starting with the fast innermost current loop, which is used to control the torque of an electrical machine, follow by the speed and position loops. As in any cascade control structure, the inner loops are added to mitigate disturbances in the controlled variable of the outer loops to improve response following and speed [2]. Therefore, the torque quality becomes an important factor in the robotics system's ability to achieve smooth, precise movement. Since if the torque control following is poor or slow, the speed and position controllers outside it will reflect this behaviour.

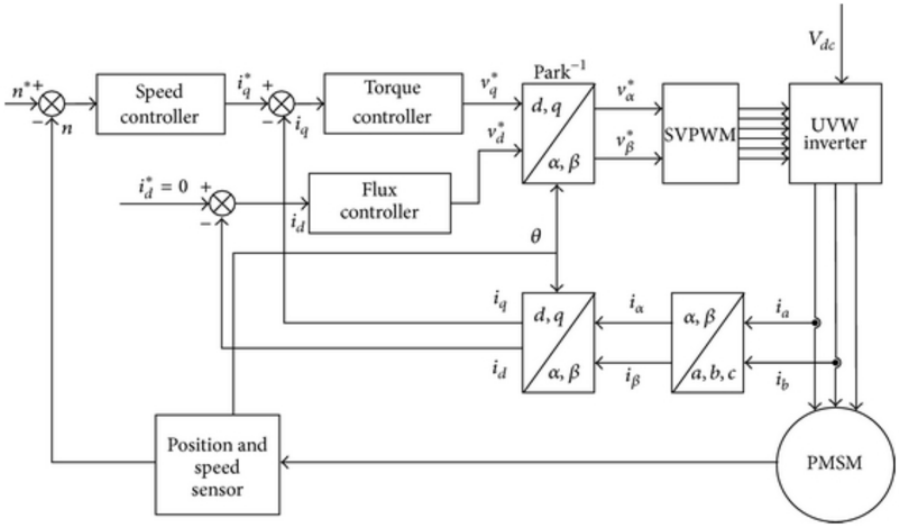

Figure 1.1: Control structure of a PMSM using field oriented control [3].

Under ideal circumstances the electric torque of the motor is converted to mechanical torque on the output shaft linearly. This however is never completely achievable in practice. Common sources of nonlinear behaviour in the torque delivery of the motor are reluctance torque and cogging torque. To minimise the contribution from these effects, changes are often made to the design of the machine, the drive system and mechanical setup. In this case however, the existing non-ideal and non-linear behaviour of the machine are the points of interest. As the main goal of the thesis is not to redesign the machine but to provide an in-depth analysis of the electrical machine, this master thesis will evaluate how the delivered torque differs from the demanded one, and then attempt to formulate a compensation. While high torque quality is required to precisely control the movement of industrial robots, this is likely to be hampered by cost and weight optimisation. System effects from friction, quantisation, vibrations, cross resonances and

coupling further complicates matters. Since the robot in general is programmed by the end user, their specific use case is often not known to the engineers when optimising the robot. It follows that the trajectories, load cycles and reference values and other process-related conditions are incomplete or not at all available. All of this in combination means that it is extremely important for the control system of each motor to accurately follow a given reference torque, for the whole work range of the robot.

In this particular instance, issues with inconsistencies in the delivered torque of the PMSM motors gave rise to vibrations in the end use. In order to explain the practical challenges, this work refers to a positioning example [4], which obviously requires a very precise position control from the control system. The issues that have been encountered were initially thought to be caused by cogging effects. After FEM analysis of the motor did not show signs of this being the case more testing had to be done. Through this testing it has been shown that torque ripple does appear but that cogging is not the main cause. Instead of the there being only one source of torque ripple as expected, there are several origins of torque ripple and pulsation that need to be investigated and analysed first. Thereafter, they can be compensated, where the added current reference used in this paper is one of the obvious options. However, as the source of the torque ripple is not that which was expected, time limitations made a thorough enough experimental evaluation of the origins of the torque ripple and pulsation to implement a proper compensation for an existing servo drive system unfeasible. As such, no compensation was implemented. A brief chapter has been included on what an initial attempt at compensation for a well modelled disturbance could look like.

Initial intention was to carry out investigations on torque ripple caused by cogging. Since the cogging was not the source of torque pulsation it became apparent that all possible sources of torque pulsation, starting from drive system, electric machine construction, and mechanical arrangement need to be explored.

1.2 Objectives

The goal of this thesis is to verify the difference between the demanded and the actual delivered torque, as well as implementing a compensation outside of the servo drive system's control loop. This is done based on the rotors mechanical position to reduce the ripple in the torque, as the suspected source at the start of the thesis was cogging. Reducing the ripple would result in a more even acceleration and reduced vibrations during load, improving the performance in general. The main focus of this work is to explore the variation of static and quasi-static torque experimentally and explain some origins of torque pulsations when studying the results of models. However, developing models is not the focus of the work.

1.3 Methodology

Both practical and theoretical methods are used to perform the evaluation. A constructed test bench is used to perform practical tests on the motor. The motor is tested both statically and quasi-statically, i.e. running with a fixed torque reference. It is also evaluated numerically using FEM software. To evaluate possible effects from the servo drive on the torque quality, a model was implemented. This model was also used to test the possibility to compensate a well known disturbance.

1.4 Limitations

Hardware limitations to set up a precise test bench for torque measurements were present during the thesis. This stemmed both from limited access to high-end measurement equipment, and building materials for the test bench. Parts of the test bench were 3D-printed in PLA (polylactic acid) plastic, which has less ideal rigidity properties than e.g. aluminium. Most of the data management of the measurements had to be done manually, as this was not an established process and therefore no automation was present to reduce the workload and save time. This thesis was done in collaboration with Cognibotics, which are not the motor manufacturers. The work is mainly experimental, which means that it was influenced by availability and accessibility of components and systems needed carrying out the measurements. Moreover, given that the torque pulsation is a result of time harmonics of the supply and the space harmonics of the machine construction, participation in power electronic control (EIEN25) and design of electrical machines (EIEN20) courses would provide a better pre-knowledge for in-depth analysis of electromagnetic vibration.

2 Theory

The theory of the subjects discussed in this thesis is presented here to help make it easier to following along with the work done in this thesis. The Clarke and Park transformations, used to obtain the d, q-reference frame, basic theory of torque production in a PMSM, the cogging torque effect and different compensations techniques for torque ripple are presented.

2.1 Cogging Torque

Cogging torque is defined as the torque produced by the motor while not under load. This is caused by the attraction between the stator teeth and the magnets in the rotor. The cogging torque can be calculated using

$$T_{cog} = -\frac{1}{2}\phi_{gap}^2 \frac{d\mathscr{R}}{d\theta} \tag{1}$$

where ϕ_{gap} is the air-gap magnetic flux, $\mathscr{R}$ is the reluctance in the air-gap and θ is the mechanical position of the rotor. From this equation it can be seen that the cogging torque will vary over the revolution of the motor, since the reluctance varies with the position. This is caused by variations in the magnetic path as the magnets on the rotor sit in different positions in relation to the stator teeth, as seen in figure 2.1. [5]

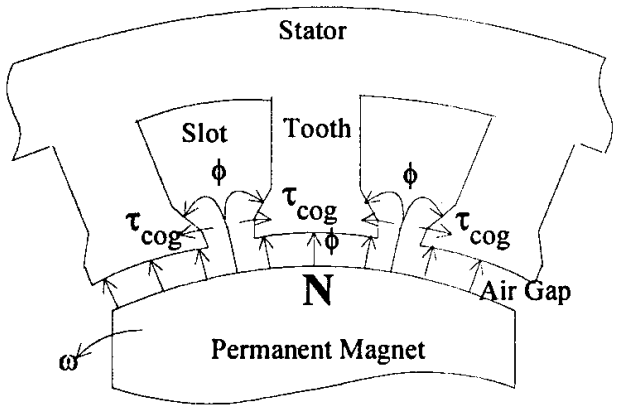

a. Net Cogging Torque Equal to Zero.

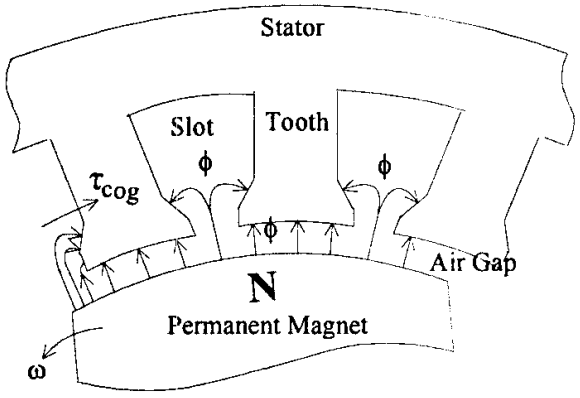

b. Net Cogging Torque Greater than Zero.

Figure 2.1: Visualisation of why the cogging torque varies over a mechanical rotation. **a.** Rotor position with symmetric magnetic attraction in both directions. **b.** Rotor position with non-symmetric magnetic attraction. [6]

This effect will periodically repeat a certain number of times over the revolution of the motor, defined by the number of magnetic poles and stator slots. For a motor with identical evenly spaced magnets along the rotor and teeth evenly spaced along the stator, the periods per mechanical revolution m, is calculated as

$$m = \text{LCM}\{Q,\, 2p\} \tag{2}$$

where LCM is the least common multiple, Q is the number of stator teeth and p is the number of pole pairs in the rotor [7],[8]. In figure 2.2 one such period can be seen, observe that this setup would have four such periods per mechanical revolutions, since $\text{LCM}\{4,\, 4\} = 4$.

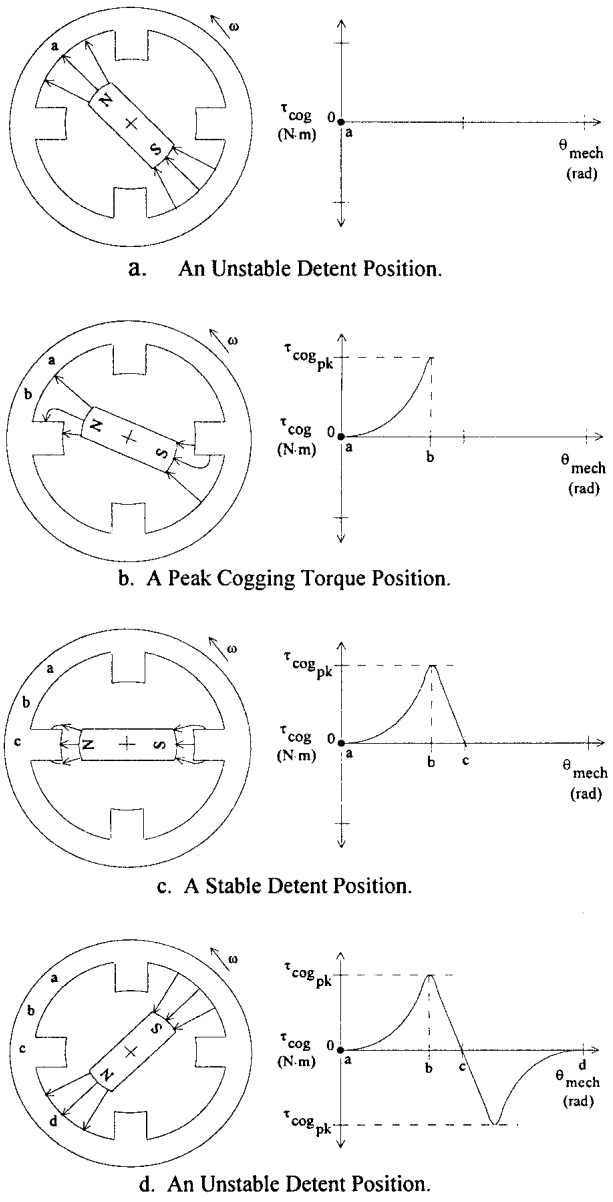

Figure 2.2: Picture of a full period of cogging for a simple motor with four stator teeth and one pole pair. [6]

2.2 Harmonic Flux

The harmonic flux is caused by fluctuations in the magnetic flux density distribution in the air-gap between the rotor and the stator or irregularities in the stator currents. In this paper the 6th harmonic is of most interest, which is commonly the case, but the equations can be applied to higher order harmonics as well. In the d, q-reference frame the currents can be expressed

as:

$$
\begin{aligned}
i_{dq} = I_{\max} \begin{bmatrix} \sin(\varphi_i) \\ -\cos(\varphi_i) \end{bmatrix} + h_{5i} \begin{bmatrix} \sin(6\omega_e t + \varphi_{5i}) \\ \cos(6\omega_e t + \varphi_{5i}) \end{bmatrix} \\
+ h_{7i} \begin{bmatrix} \sin(6\omega_e t + \varphi_{7i}) \\ -\cos(6\omega_e t + \varphi_{7i}) \end{bmatrix}
\end{aligned} \tag{3}
$$

where I_{max} is the amplitude of the fundamental harmonic, φ_i is the phase shift of the respective harmonics, h_{5i}, h_{7i} are the amplitudes of the 5th and 7th harmonics respectively and ω_e is the electrical speed. [9]

Looking at the equation, it can be seen that both the 5th and 7th harmonics have a frequency of six times that of the fundamental electrical frequency. This is caused by the Clarke and Park transformation, presented in more detail in 2.3, transforming the standard a, b, c-reference frame to the d, q-reference frame. For an intuitive explanation it can be said that when viewing the system in the d, q-reference frame we are following along with the fundamental frequency, essentially removing it from view. This expresses itself as reducing the 5th and 7th harmonics one degree, resulting in the positive and negative 6th harmonic, as the 5th is actually a negative harmonic.

2.3 Drive System and Current Control

This section presents the theory of how the control of the current is set up and how the motor currents produce torque.

Clarke and Park Transformations

When talking of the currents running through the motor, they are referred to as the i_q and i_d currents. The phase currents usually referred to as the A,B,C-currents are transformed into alpha,beta-currents using Clarke transformation which are further transformed into the d,q-currents using Park transformation [10]. After these transformations we are left with this representation of the voltages [11]

$$
\begin{aligned}
u_d &= L\frac{d}{dt}i_d + Ri_d - \omega L i_q + e_d \\
u_q &= L\frac{d}{dt}i_q + Ri_q - \omega L i_d + e_q
\end{aligned} \tag{4}
$$

where L is inductance, i is current, R is resistance, ω is rotational speed and e is the back emf.

Torque Production

The torque produced by a general synchronous motor can be calculated as

$$
T = p \cdot \psi_m \cdot i_q + (L_d - L_q) \cdot i_d \cdot i_q \tag{5}
$$

where p is the number of poles, ψ_m is the magnetic flux linkage, i_q is the quadrature current, i_d is the direct current, L_q is the quadrature inductance and L_d is the direct inductance. For a

permanent magnet synchronous motor in particular i_d is controlled to zero, as well as the motor construction aiming for $L_d - L_q = 0$. Assuming that either of these are truly zero 5 can be simplified as:

$$T = p \cdot \psi_m \cdot i_q \tag{6}$$

Resulting in a linear relationship between the i_q-current and the torque, T. This is then used to control the torque.

2.4 Impact of Drive System

There are many possible sources of non-ideal behaviour originating from the drive system. Some of these are presented in

Pulse Width Modulation

To effectively control a voltage, a commonly used technique is pulse width modulation, often referred to as PWM. Using a source with a set voltage the output can be reduced by using transistors that switch between being on or off, so that the average voltage reaches a desired value. This technique however has the inherent effect of causing a ripple in the output, which can lead to adverse effects on the motor behaviour. This can be mitigated by synchronising the current sampling to the switch frequency so that the sampling occurs when the average and actually value coincide. This occurs at the beginning of and at the halfway point of a cycle. [12]

Inverter Dead Time

In ideal inverter bridges the transistor gates are assumed to switch instantaneously and symmetrically, i.e. no time difference between turning off one transistor and then on the other in the same phase leg of a 2-level converter. In practice however this cannot be guaranteed. This can lead to a short circuit if the transistor that is meant to turn off is slower than the one that is turning on, as both would be on at the same time. To alleviate this, dead time is added when turning on a transistor, ensuring that the other has time to turn off. This causes a short time-span where both transistors are turned off. These effects can lead to excitations of the 5th and 7th harmonics in the servo system. [13] [14]

2.5 Impact of Mechanical System

A mechanical system, such as the one built to measure the torque of the motor in this thesis, will always have certain imperfections in its construction in reality. These imperfections can be described and identified through frequency analysis. The most relevant imperfections in the context of this thesis are misalignment and mechanical looseness. Connections between axis are done using couplers to alleviate some of the effects of misalignment, which appear as spikes in the frequency analysis at twice the rotational speed of the axis. Mechanical looseness is caused by components not being fastened well enough or a lacking stiffness of the components. These effects cause spikes correlating to whole or half multiples of the rotational speed, ranging from two to ten times faster than the rotation. [15]

2.6 Compensation Techniques

This section will discuss different compensation techniques that can be applied to minimise pulsation in the torque output of a motor. These techniques can be divided into two categories; motor design based and control based.

Machine Design Based Compensation

There are quite a few adaptions possible in the machine design that affects torque pulsation. In general though, these techniques focus on minimising the cogging torque of the motor. As changes to the design of the machine are not within the scope of this thesis, some methods will be mentioned but not explained in detail. Machine design based techniques include; optimal pole arc [7][16][17], magnet shifting [7][16], magnet and stator skewing [16][17] and dummy slots and teeth [16], among others.

Control Based Compensation

Feedforward is implemented to handle any sort of measurable disturbance before it shows up in the output signal, in this context the torque. By mapping out the pulsations of the torque in regard to some variable or variables, the inverse of these undesired effects can be applied to the signal with the goal to cancel them out. These variables could be e.g. position of the rotor, speed or magnitude of the current [2]. It is also possible to apply the same fundamental idea to more sophisticated solutions, such as the one purposed by Prof. Ferretti, Dr. Magnani and Dr. Rocco in [18].

Harmonic injected current is used to minimise periodic pulsation effects in the torque by shaping the phase current. This is achieved by adding one term to the i_q current for each harmonic one wishes to suppress. To calculate the injected current, the following equation is used

$$i^c_{q,n} = -\frac{2T_{cm,n}}{6p\psi_m} cos(6n2p\theta_r + \varphi_{cog,n}) \tag{7}$$

where n signifies the number of the harmonic of the fundamental frequency to be cancelled, $T_{cm,n}$ is the magnitude of the harmonic, p is the number of pole pairs, ψ_m is the flux-linkages of the permanent magnet, θ_r is the rotors angular position and $\varphi_{cog,n}$ is the phase shift of the cogging torque.[16][19][20]

Speed loop disturbance rejection uses a fundamentally different approach to the problem. Instead of attempting to improve upon the quality of the delivered torque, it is left to the speed loop surrounding the torque loop to handle any irregularities in the torque. This technique is however only suitable for lower motor speeds where the loop speed of the torque loop falls well within the bandwidth of the speed loop.[16]

3 Method

This section present the methods used to perform the torque measuring of the system. The intent is for the work to be repeatable and to allow for assessment of how well chosen the methods are for the goals of this thesis.

3.1 Quasistatic Method

Two different measurement methods are used to evaluate the torque ripple of the motor. In the first set of measurements the motor is allowed to spin freely in a torque control configuration with different torque references. Eight different torque references are used in this method, 64, 70.4, 76.8, 80, 83.2, 86.4, 89.6 and 92.8 Nmm. The lowest reference was chosen since it is the least amount of demanded torque that made the motor spin reliably. The highest was chosen as to not risk damaging the motor or test bench. The step size between these originates from how the references are referred to in the code, where per mille of rated torque is used. The references in per mille are 100, 110, 120, 125, 130, 135, 140, 145. Initially the intention was to use a step size of 10 per mille, but this was deemed too large since the speed of the motor do not increase linearly with the reference torque. The purpose of these measurements is to identify any possible variations of the torque over the electric revolution of the motor. This is done by plotting the torque over the mechanical angle of the rotor.

3.2 Static Method

In the second measurement method, the motor is instead fixed in different positions and the torque reference varied in these positions. The same test bench is used in both configurations, with the exception of the part used to lock the motor in position that is used in the second test. Position, torque, currents (I_q and I_d) are measured, and the speed is calculated. The torque reference as well as the torque calculated by the controller are also recorded. The positions used are based on the motor's encoder, using the zero point of the encoder as position zero for the measurements. Measurements are then taken at 10 mechanical degree increments, up to 90 degrees. The measurement positions are referred to as "P" followed by its increment numeral, counting from position 0 at 0 degrees ($P0$), up to position 9 at 90 degrees ($P9$). These measurements are made to confirm that any potential torque variations observed with the motor rotating are indeed due to the rotors position at that instant and not some other underlying reason.

3.3 Compensation Method

To compensate the irregularities in the torque output, a suitable technique needs to be chosen. Among the ones presented in the theory section, only a feed forward solution is fitting within the constraints of the thesis. As mentioned before, design changes to the motor is not of interest, meaning the most commonly applied solutions to cogging torque issues are not applicable. The driver is not redesign-able either, excluding the harmonic current injection technique. Lastly because of the motors intended use in a robotic arm it is not feasible to assume that the speed loop can be left to take care of any issues in torque delivery.

4 Experimental Evaluation Platform

The specifications of the motor, driver and measurement equipment is presented here. It is also explained how the test bench that was used to perform the tests is set up and what software was used in the context of recording the measurements.

4.1 Test Objects

The motor is the main object of review in this thesis, but since the drive unit is an important part of its behaviour it too is included. Their specifications are presented here.

Motor

The motor being evaluated is an AC PMSM servo motor. The specifications of the motor are presented in table 4.1, along with measured inductances in table 4.2.

Table 4.1: Shows the specifications of the tested motor.

RPM	**Power**	**Torque**	**Current**	**Voltage**	**Frequency**
3000	0.2 kW	0.64 Nm	1.9 A	AC 200 V, 3∼	200 Hz

Table 4.2: The measured inductances of the tested motor.

Connection	1-2	2-3	1-3	1-23	3-12	2-13
Inductance at 0.2 Hz [mH]	12.7	12.7	12.7	9.49	9.43	9.52

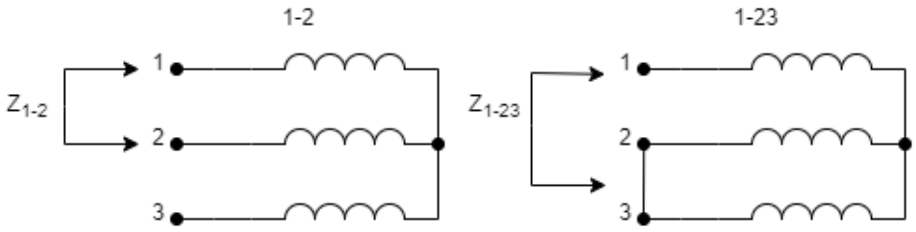

Figure 4.1: Picture showing two examples of how the measurements in table 4.2 were taken.

Driver

The specifications of the servo drive unit can be seen in table 4.3.

Table 4.3: Shows the specifications of the driver used.

	AC-input	**AC-output**
Voltage	200-230 V	0-200 V
Frequency	50/60 Hz	0-300 Hz
Current	3.7 A	2.8 A
Power	N/A	0.4 kW

4.2 Test Bench

The test bench was constructed by attaching the different components to a rectangular piece of aluminium with the dimensions 120x500 mm. The components used for the measurements are, listed in order from left to right, the motor, a torque transducer and an inertia element. For the static test a locking mechanism at the end of the inertia element is also used. The components are attached to each other using Oldham styled couplings. These are chosen because of their competitive price, accessibility and small size. There are other types, such as disk couplers, that would provide a better torque transmission but with the limited magnitude of the torques involved and the more prohibiting size of solutions using off the shelf components, the Oldham couplings were deemed sufficient [21].

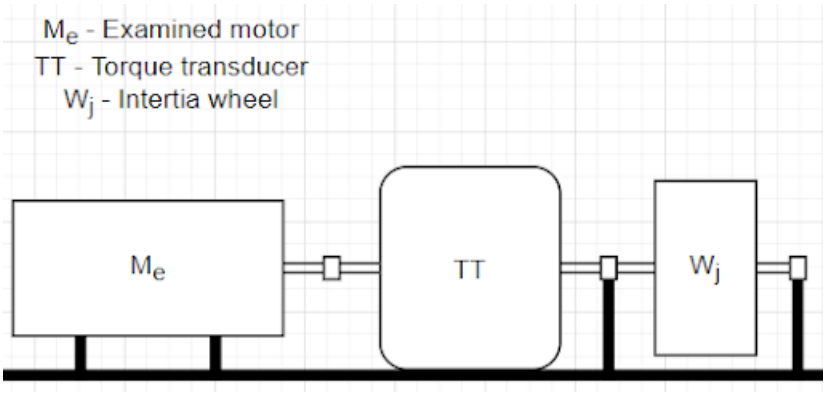

Figure 4.2: Schematic representation of the test bench used for the tests.

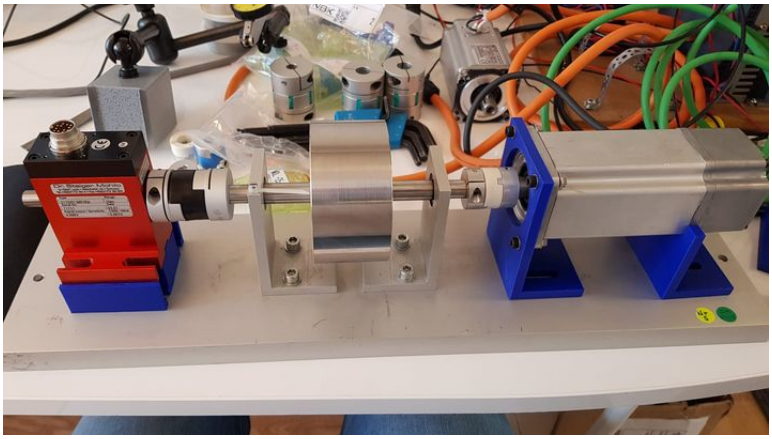

Figure 4.3: Photo of the test bench. This photo was taken to compare sizes and positioning, the order used for the actual testing is shown in figure 4.2.

4.3 Measurement Equipment

The motor position is measured using an encoder with a 32 bit resolution that is then recalculated to the motors absolute position in radians. The final resulting resolution is about $1.46 \cdot 10^{-9}$

radians.

The torque is measured using a torque transducer with a measuring range of 1 Nm, called 0170 MS 1 RAU of the brand Dr. Staiger Mohilo. The output voltage is then digitised using an EL3002, Beckhoff unit, with 12-bit resolution.

For the i_q and i_d currents the internal measurements of the servo system are used, which are implemented using resistive current measurement. The current measurement components used by the manufacturer are not know in detail, making an evaluation of the reliability of these measurements not possible.

4.4 Software

For the torque and the position measurements, as well as the calculations of the velocity, TwinCAT is used. For this thesis the motor is run in torque control mode using the manufacturers implemented control. The software used to record the current measurements is made by the servo manufacturer themselves. It is limited to recording 1000 samples at a time on two to four channels, depending on what is being measured. The data is the handled in Matlab, which is used for presentation and processing.

5 Model Based Evaluation Platform

In this chapter the model based work is presented. This work is done to evaluate the effects of the driver, cogging as well as the magnetic properties of the motor and their effects. First a simulation of the ideal case is run and analysed, then a disturbance is introduced, which is then compensated for. The worst case scenario of using the same compensation method is also included as a cautionary tale. In the magnetisation simulations two possible issues are evaluated, the effects of different rotor magnetisations and an imperfection in the stator manufacturing.

5.1 Driver Modelling

For modelling of the drive system of the test setup a slightly modified version of a modelled used in the course Power Electronics (EIEN25) is utilised [22]. The model is constructed using Simulink and is shown in figure 5.1.

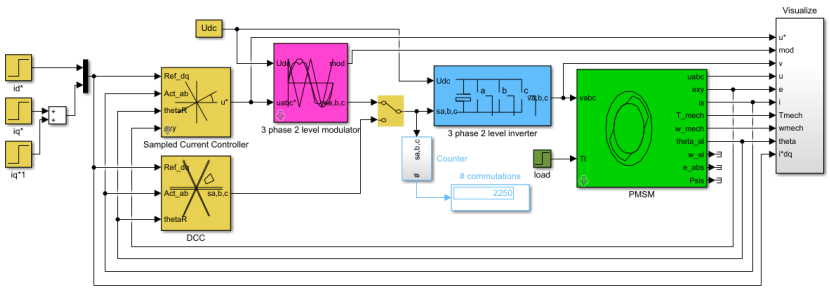

Figure 5.1: Overview of the Simulink model used.

In the model a few constants needs to be defined to run the simulation, these constants, their values and their meaning are as follows; $Rs = 2.4$ the stator resistance, $p = 8$ the number of poles, $Lsx = Lsy = 6.4 \cdot 10^{-3}$ the inductance in the x- and y-directions respectively, $Psim = 0.0572$ the magnetic flux linkage, $Udc = 200$ the direct voltage, $J = 0.2 \cdot 10^{-3}$ the inertia of the rotor, $di = 0.2$, $Ts = 1/25 \cdot 10^3$ the switching time, $Ismax = 3.2$ the maximum stator current, $Iqref = 0.8112$ the reference for the i_q current and $n0 = 1000$ the initial speed of the motor.

Ideal Motor

The first step in the modelling is to model the behaviour of the motor and drive in ideal conditions. The results of this simulation can be seen in figure 5.2, 5.3 and 5.4.The time-frame of the torque measurement is chosen to show the switching behaviour seen in the model, this is matched in the second further zoomed in current figure. The time-frame of the first picture of the current simulation is about one electric revolution.

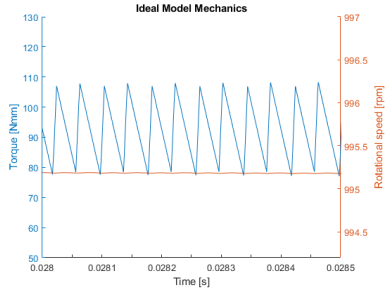

Figure 5.2: Torque (blue) and rpm (orange) of the ideal simulated motor and driver.

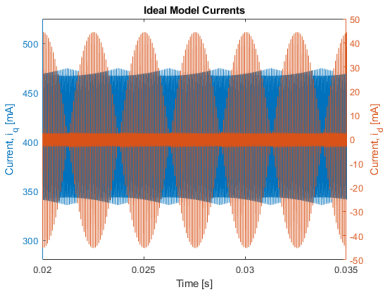

Figure 5.3: i_q current (blue) and i_d current (orange) of the ideal simulated motor and driver.

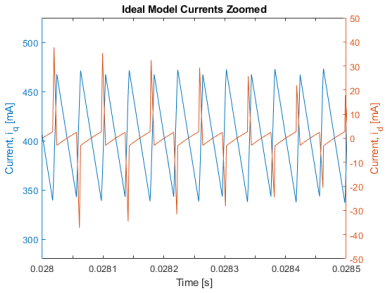

Figure 5.4: i_q current (blue) and i_d current (orange) of the ideal simulated motor and drive, further zoomed in on the time axis, to show the effect of switching.

Real Motor

A disturbance is introduced to the system, in the form of a sinusoidal signal added to the torque, with a frequency of six times per electrical revolution, or 24 per mechanical. The simulation results of this is shown in figure 5.5 and 5.6. Observe that the time-frame of the figure showing the mechanical simulation results is significantly longer than that of figure 5.2.

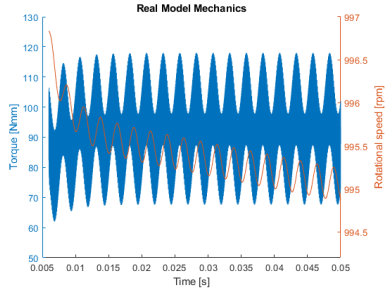

Figure 5.5: Torque (blue) and rpm (orange) of the simulated motor and driver with introduced disturbance.

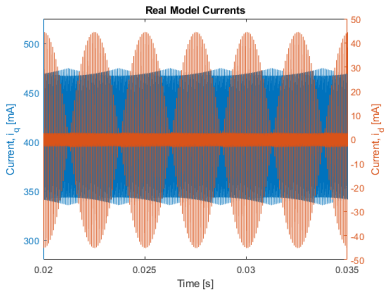

Figure 5.6: i_q current (blue) and i_d current (orange) of the simulation with introduce disturbance.

Compensated Motor

Then an attempt to compensated for the introduced disturbance is made by applying the corresponding i_q current to cancel out the effect. This is done using the same frequency as the disturbance, and the magnitude of the current is calculated using equation 6.

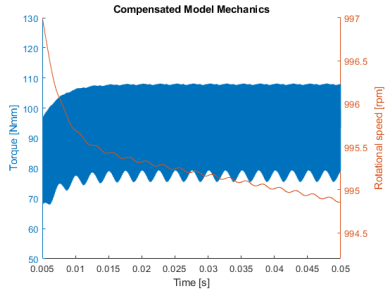

Figure 5.7: Torque (blue) and rpm (orange) of the simulated motor and driver with the disturbance compensated for.

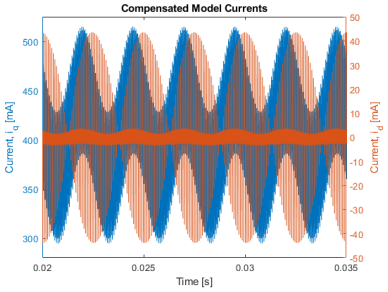

Figure 5.8: i_q current (blue) and i_d current (orange) of the simulation with the disturbance compensated for.

Worst Case Compensation

Using such a rudimentary approach to solving the issue might seem straight forward and simple, which it is in theory. Another simulation was therefore made to show the risks of such an approach. In figures 5.9 and 5.10 results are shown of simulation where the compensation is misplaced by π radians, or simply with the incorrect sign, which would be the worst case scenario for this approach.

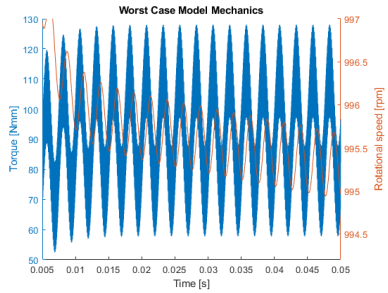

Figure 5.9: Torque (blue) and rpm (orange) of the simulated motor and driver where the compensation causes the worst case scenario.

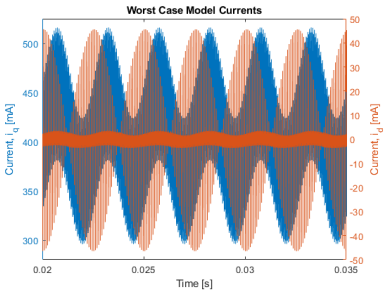

Figure 5.10: i_q current (blue) and i_d current (orange) of the simulation motor where the compensation causes the worst case scenario.

5.2 FEM Analysis

This section presents the FEM analysis made of the motor, which is done to analyse the cogging torque and the magnetic properties. The FEM analysis is made using two different software tools, FEMM and Ansys. FEMM uses a static model and is here used to simulate the effects of different magnetisations of the rotor. Ansys is a transient model used to analyse cogging torque and the torque ripple due to iron losses with and without a stator gap.

In figures 5.11-5.14 two different kinds of magnetisation techniques of the rotor magnets are shown, both are simulated when the motor is unloaded and loaded ($i_d = 0$ and different i_q values tested, see figure 5.17). These are diametrically magnetised (DM) and radially magnetised (RM). This simulation is run such that the motor is tested statically in different positions.

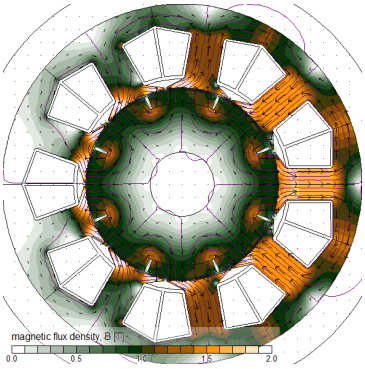

Figure 5.11: No load applied, diametrically magnetised magnets.

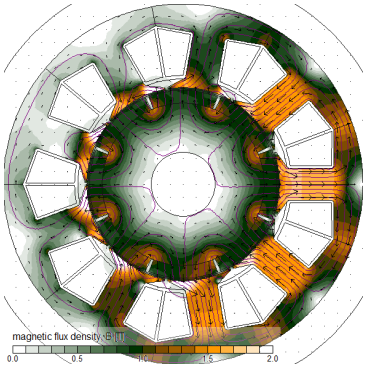

Figure 5.12: Load applied, diametrically magnetised magnets.

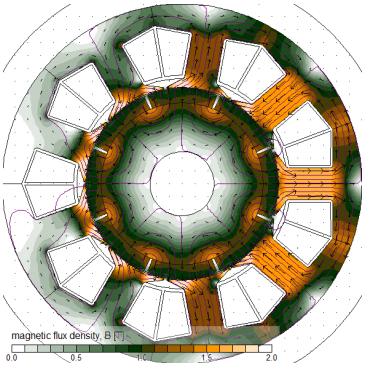

Figure 5.13: No load applied, radially magnetised magnets.

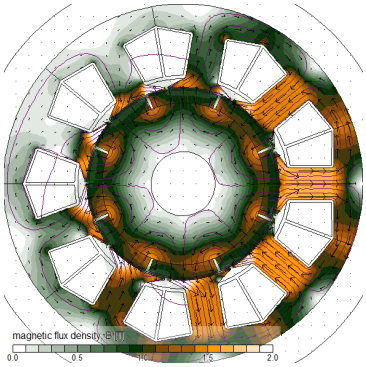

Figure 5.14: Load applied, radially magnetised magnets.

The two rotor configurations in figures 5.11-5.14 are then implemented in a simulation that shows the effects of the stator current on the torque output, in different rotor positions. The motor is simulated to be static in these positions. The results of these simulations can be seen in figures 5.15-5.17. Observe that although left out because of limited space, the convention of line showing RM and "dashed and plus-sign" corresponding to the DM still holds in figure 5.17. As the cogging

torque is defined as the torque variation at zero current, it can be seen in these figures that it should be as low as 1 Nmm.

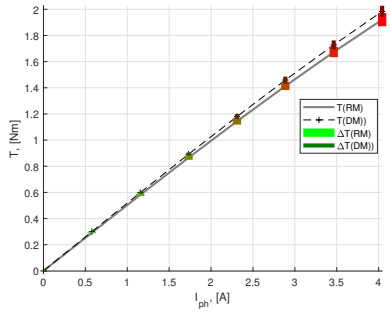

Figure 5.15: Comparison of the torque produced with radially and diametrically magnetised rotor magnets.

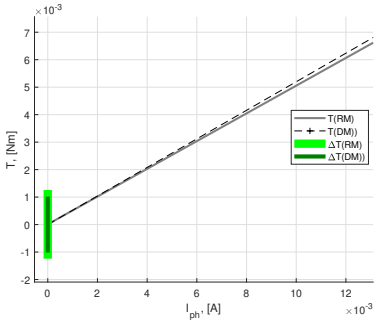

Figure 5.16: More zoomed in to show the variation at 0 A

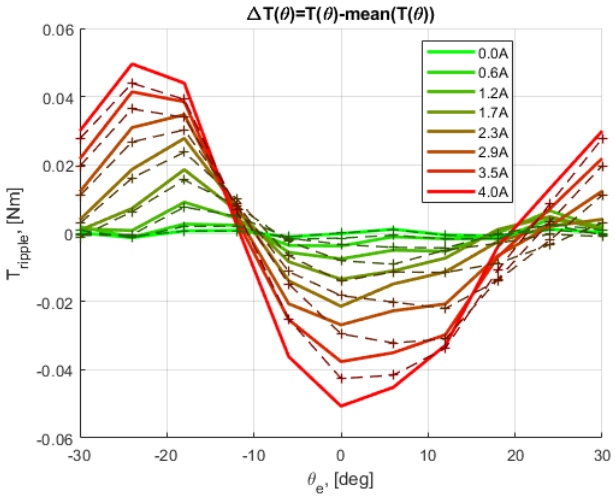

Figure 5.17: Shows how the torque ripple varies with electrical position as well as current.

In figures 5.19-5.22 the effects of a potential air gap in the stator is simulated. This is usually caused by imperfect manufacturing. Figure 5.18 Shows a close up of the gap simulated. The gap is locked between the two stator pieces marked in pink.

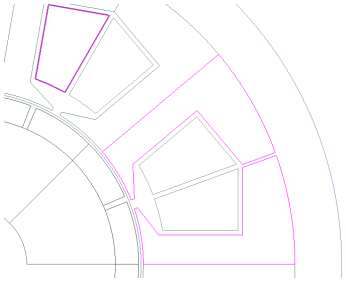

Figure 5.18: 0.25 mm stator gap.

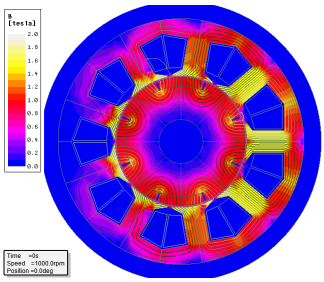

Figure 5.19: Flux density without stator gap.

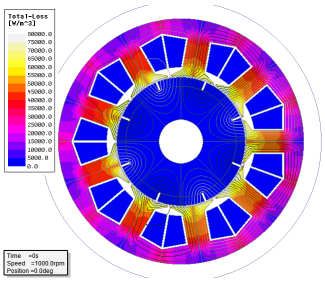

Figure 5.20: Loss density without stator gap.

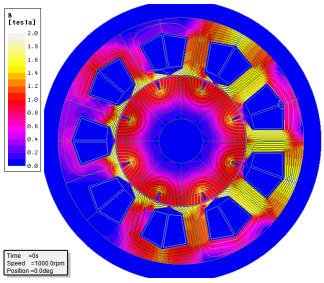

Figure 5.21: Flux density with stator gap.

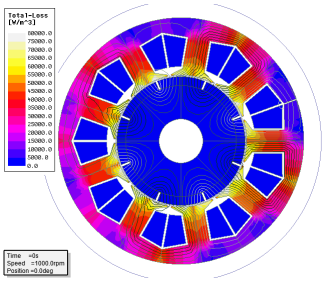

Figure 5.22: Loss density with stator gap.

The impact of the flux and loss density shown in figures 5.19-5.22 are then simulated over one electric revolution, using the program Ansys. In figure 5.23 a fluctuation in torque can be seen with a period of two per electrical rotation. In figure 5.24 to large loss spikes can be seen, also twice per rotation.

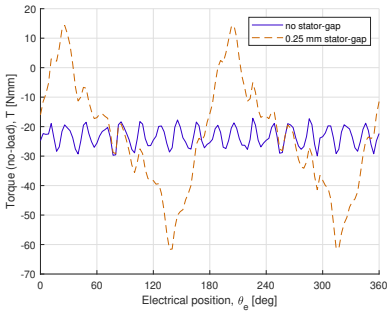

Figure 5.23: Simulated torque over an electrical revolution, with and without a stator-gap present.

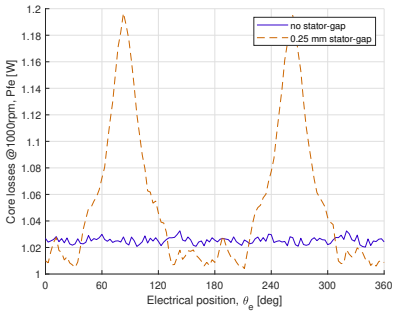

Figure 5.24: Simulated core losses over an electrical revolution, with and without a stator-gap present.

An overview of the effects shown on the torque by the FEM analysis is also produced to make comparing them easier. It can be seen in table 5.1.

Table 5.1: Overview of FEM torque results.

	Amplitude [Nmm]	**Frequency per electric revolution**	**Frequency per mechanical revolution**
Magnetic saturation, figure 5.17	± 10	6	24
Flux density no gap, figure 5.23	± 5	18	72
Flux density with gap, figure 5.23	± 40	2	8

6 Measurement Results

In this section the different measurement results are presented. The first sub-chapter presents the results from the quasi static tests. Both raw measurements and spectral analyses are included, as well as some explanations of the results. The second sub-chapter shows the results from the static tests also including spectral analyses and explanations. The sub-chapters themselves are further divided into torque and current measurements.

6.1 Quasi Static Tests

The first measurements are obtained using the quasi static method. A schematic overview of the test set up can be seen in 6.1. In this figure T_{ref} is the torque reference, T_{em} is the electromagnetic torque, P_{loss} is the power loss, w_{el} is the rotational speed in the electrical reference frame, TT is the torque transducer, J is the inertia of the fly wheel, s is the Laplace variable, b is the dampening of the rotation and w_m is the speed of the mechanical rotation.

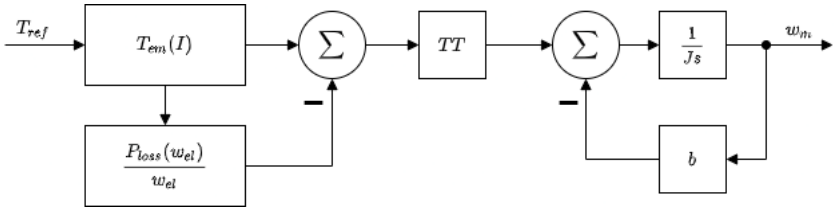

Figure 6.1: Schematic of the quasi static test set up.

In table 6.1 a summary of the measurement results from the quasi static tests is presented. T_{ref} is the reference torque used for that test, I_q is the quadrature current, f_{el} is the number of electrical rotations per second, T_{meas} is the torque measured by the torque transducer, T_{calc} is the ideal torque calculated as calculated by the driver supplier, w_m is the mechanical rotational speed of the motor and P_{loss} is calculated as $(T_{ref} - |T_{meas}|) \cdot w_m$. The values following the $\pm$-signs are calculated as half the difference between the maximum and the minimum of the relevant measurement, e.g. $\frac{1}{2}(max(I_q) - min(I_q))$. All other values in the table are mean values.

Table 6.1: Overview of the measurements from the quasi static tests.

	T_{ref} $[Nmm]$	I_{ref} $[mA]$	I_q $[mA]$	f_{el} $[Hz]$	T_{meas} $[Nmm]$	T_{calc} $[Nmm]$	w_m $[rpm]$	$P_{loss}(w)$ $[W]$
Test 1	64.0	280.0	281.6 ± 41.25	5.0	3.7 ± 10.4	64.4 ± 9.4	74.5 ± 4.3	0.47
Test 2	70.4	307.5	305.9 ± 43.75	10.1	6.5 ± 8.5	69.9 ± 10.0	151.4 ± 6.4	1.01
Test 3	76.8	335.0	335.3 ± 36.25	18.2	9.5 ± 6.1	76.7 ± 8.3	272.9 ± 10.5	1.92
Test 4	80.0	350.0	349.4 ± 40.0	22.3	11.0 ± 6.7	79.9 ± 9.1	334.8 ± 17.0	2.42
Test 5	83.2	365.0	365.0 ± 45.0	29.4	13.3 ± 5.6	83.5 ± 10.3	440.5 ± 5.6	3.23
Test 6	86.4	377.5	377.8 ± 47.50	37.0	15.3 ± 5.9	86.4 ± 10.9	554.2 ± 6.7	4.13
Test 7	89.6	392.5	391.8 ± 53.75	45.9	17.5 ± 6.2	89.6 ± 12.3	688.1 ± 16.9	5.19
Test 8	92.8	405.0	404.9 ± 38.75	56.0	19.7 ± 5.3	92.6 ± 8.9	839.2 ± 19.1	6.42

Torque Measurements

Torque measurements using the quasi static method. In figures 6.2 and 6.3 the measurements can be seen with no post-processing applied other than assigning the appropriate units to the

axis.

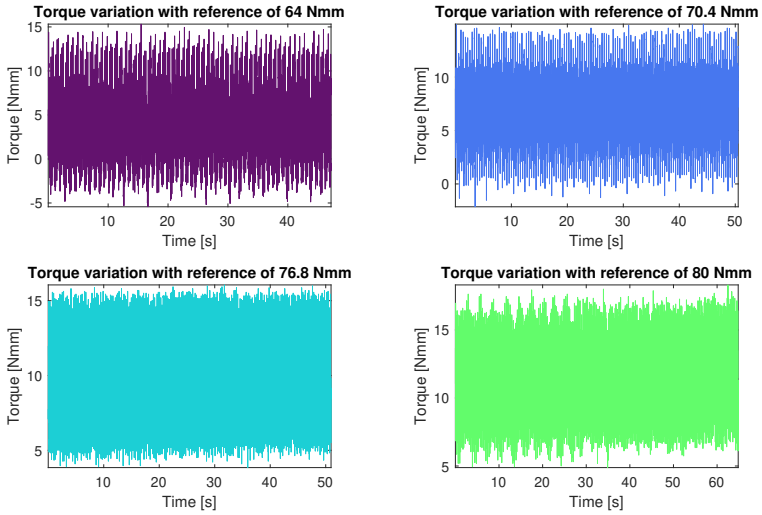

Figure 6.2: Variation in torque output of the motor for the whole measuring duration for torque references of 64, 70.4, 76.8 and 80 Nmm.

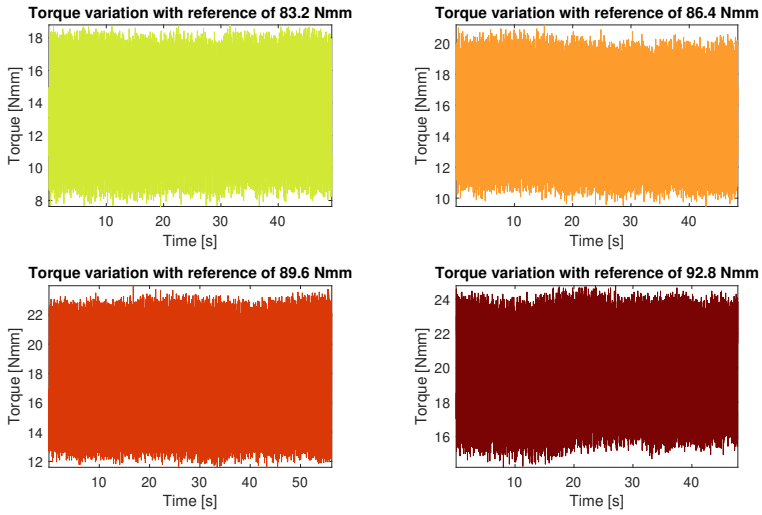

Figure 6.3: Variation in torque output of the motor for the whole measuring duration for torque references of 83.2, 86.4, 89.6 and 92.8 Nmm.

To aid in analysing the data is presented with some post-processing applied. The left halves of figures 6.4-6.11 show the measured torque periodized over the mechanical rotation, with the intent to relate variations in torque to the position of the rotor. On the right, a custom spectral analysis of the torque from the same test can be seen. The x-axis has been rescaled to "per

revolution" instead of the standard unit of Hz. This is done by dividing the frequency values of the x-axis with the speed of the measurement, in radian per second. This is done to make it easier to compare the different measurements. The x-axis of the spectral analyses is done in the logarithmic scale to fit more information and starts at 0.03 times per revolution. For finding spikes in the FFTs the Matlab function "findpeaks" is used with "MinPeakHeight" set to 1/2 Nmm for the first two measurements then to 1/3 Nmm and "MinPeakDistance" set to 50. Spikes found in this way are marked with an x in the spectra. The minimum peak height used to trigger a spike detection is set higher for the first two, as their spectra are significantly more noisy. This reduced the amount of spikes registered, avoiding many which could be classified as false positives. The setting of 50, used in "MinPeakDistance" refers to samples, for reference the FFT of the first measurement includes 94433 samples. This value is chosen somewhat arbitrarily through trial and error.

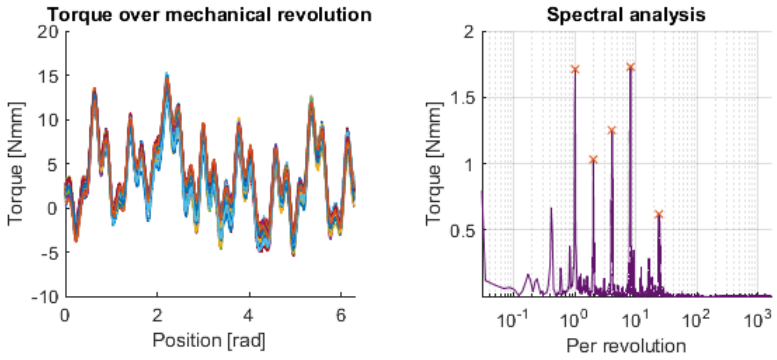

Figure 6.4: Variation in torque output of the motor over a mechanical rotation, for a reference torque of 64 Nmm, as well as the rescaled FFT of the same measurement.

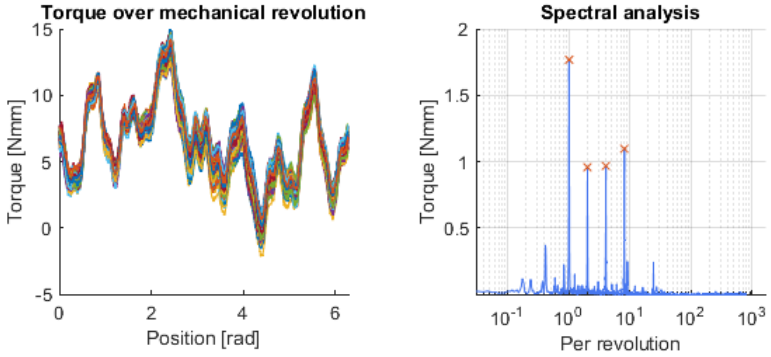

Figure 6.5: Variation in torque output of the motor over a mechanical rotation, for a reference torque of 70.4 Nmm, as well as the rescaled FFT of the same measurement.

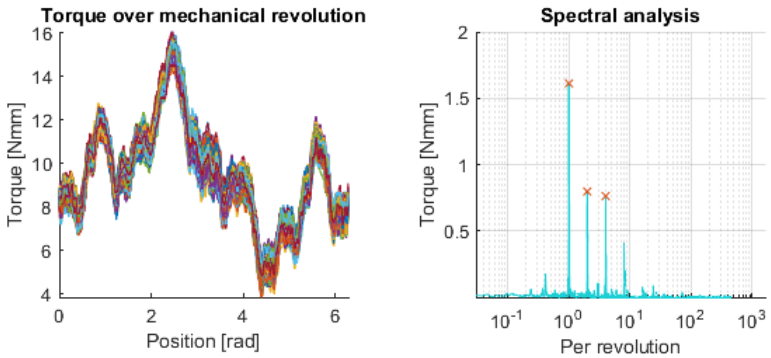

Figure 6.6: Variation in torque output of the motor over a mechanical rotation, for a reference torque of 76.8 Nmm, as well as the rescaled FFT of the same measurement.

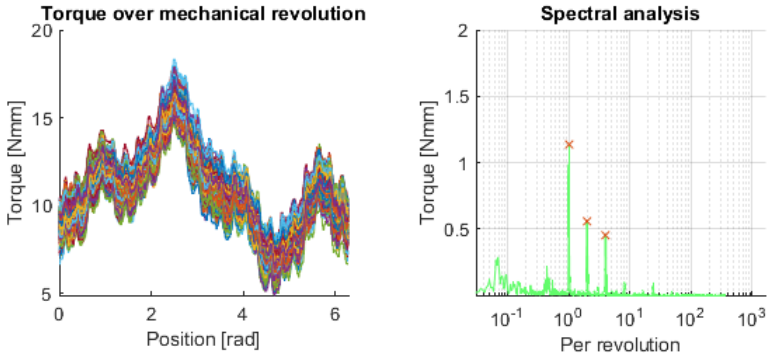

Figure 6.7: Variation in torque output of the motor over a mechanical rotation, for a reference torque of 80 Nmm, as well as the rescaled FFT of the same measurement.

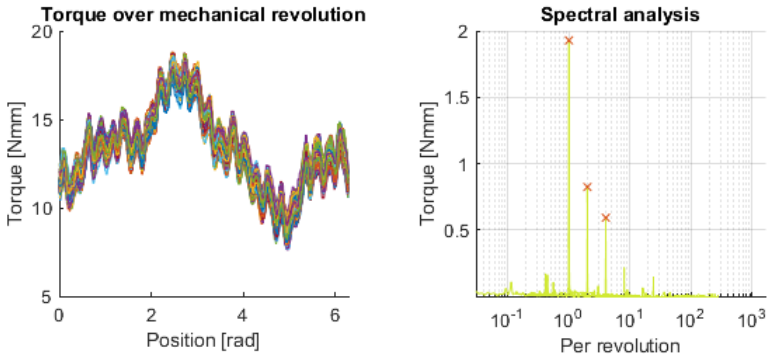

Figure 6.8: Variation in torque output of the motor over a mechanical rotation, for a reference torque of 83.2 Nmm, as well as the rescaled FFT of the same measurement.

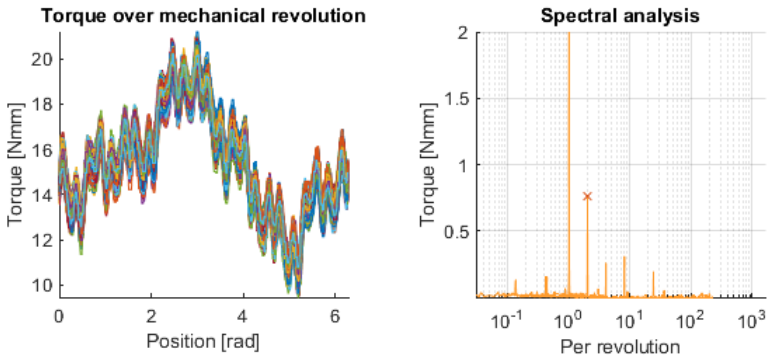

Figure 6.9: Variation in torque output of the motor over a mechanical rotation, for a reference torque of 86.4 Nmm, as well as the rescaled FFT of the same measurement.

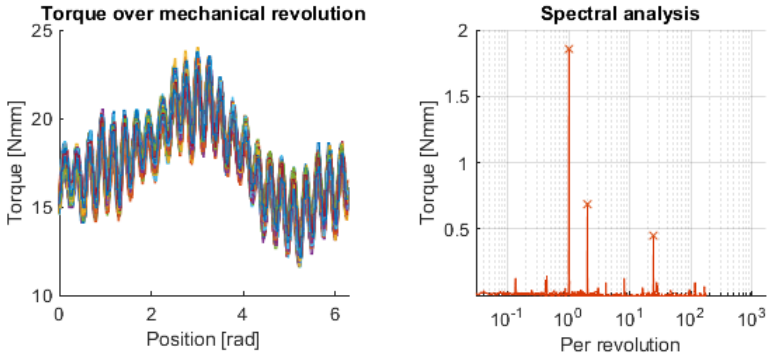

Figure 6.10: Variation in torque output of the motor over a mechanical rotation, for a reference torque of 89.6 Nmm, as well as the rescaled FFT of the same measurement.

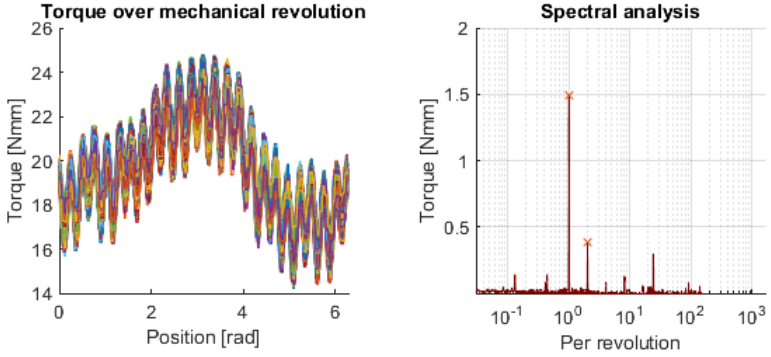

Figure 6.11: Variation in torque output of the motor over a mechanical rotation, for a reference torque of 92.8 Nmm, as well as the rescaled FFT of the same measurement.

An overview of the different spikes that corresponds to a certain number of repetitions per rotation found in the spectral analyses is presented in 6.2. Here the spikes corresponding to one, two, four, eight and twenty-four repetitions are presented, as they were deemed to be of the most interest. Even though they are not significant for all measurements, they are included for comparison.

Table 6.2: Overview comparing the different torque values from spikes repeated over the mechanical revolution.

	64 Nmm reference	**70.4 Nmm reference**	**76.8 Nmm reference**	**80 Nmm reference**	**83.2 Nmm reference**	**86.4 Nmm reference**	**89.6 Nmm reference**	**92.8 Nmm reference**
Once per revolution [Nmm]	1.711	1.768	1.612	1.136	1.929	2.002	1.856	1.491
Twice per revolution [Nmm]	1.031	0.958	0.797	0.557	0.824	0.761	0.686	0.385
Four times per revolution [Nmm]	1.251	0.970	0.763	0.452	0.592	0.255	0.092	0.08
Eight times per revolution [Nmm]	1.730	1.097	0.406	0.096	0.213	0.306	0.124	0.122
Twenty-four times per revolution [Nmm]	0.619	0.240	0.084	0.091	0.142	0.190	0.449	0.293

In table 6.3 an overview of spikes in Hz is presented. Some of the spikes are marked with an asterisk (*), these are not registered by the "findpeaks" function, but were deemed interesting and distinct nonetheless. Many of the measurements also show spikes at very low frequencies (<0.025 Hz) these are not included as they are assumed to be part of the 0 Hz spike which is not of interest.

Table 6.3: Overview of the spectral analysis results. Average rotational speed during each measurement is included for comparison.

	64 Nmm reference	**70.4 Nmm reference**	**76.8 Nmm reference**	**80 Nmm reference**	**83.2 Nmm reference**	**86.4 Nmm reference**	**89.6 Nmm reference**	**92.8 Nmm reference**
Mechanical Rotation [Hz]	1.24	2.52	4.55	5.58	7.43	9.24	11.47	13.99
Spike 1 [Hz]	1.25	2.53	4.53	5.61	7.34	9.25	11.47	14.04
Spike 2 [Hz]	2.48	5.047	9.05	11.01	14.65	18.52	22.97	28.07
Spike 3 [Hz]	4.96	10.11	18.09	22.01	29.35	37.0 *	45.9 *	56.1 *
Spike 4 [Hz]	10.06	20.25	36.2 *	44.0 *	58.8 *	N/A	275.60	N/A
Spike 5 [Hz]	29.33	N/A	N/A	N/A	N/A	N/A	N/A	N/A

Looking at the data presented in table 6.3 it can be seen that there is a spike matching one, two and four multiples of the mechanical frequency for every measurement. For a few there is also a spike matching the 8th multiple. There are two outliers as well, one from the 64 Nmm reference, with a spike at 29.33 Hz and one from the 89.6 Nmm reference at 275.6 Nmm. Both of these match-up with 24 repetitions per rotation.

Current Measurements

The current measurements taken during the quasi static tests are presented here. In figures 6.12-6.19 the raw quadrature current plot can be seen on the left and the spectral analysis on the

right, using a logarithmic x-axis. The spikes mark with X's are presented in the overview of the data shown in table 6.4. As before in the spectral analysis of the torque measurement, the Matlab function "findpeaks" is used with the options "MinPeakHeight" and "MinPeakDistance" activated. This time using 4 mA and 1 sample respectively. Observe that in this case there is only 1000 samples and because of this they have not been plotted against the position as the torque measurement are. To compare this data with the torque measurements the data presented in table 6.3 is useful.

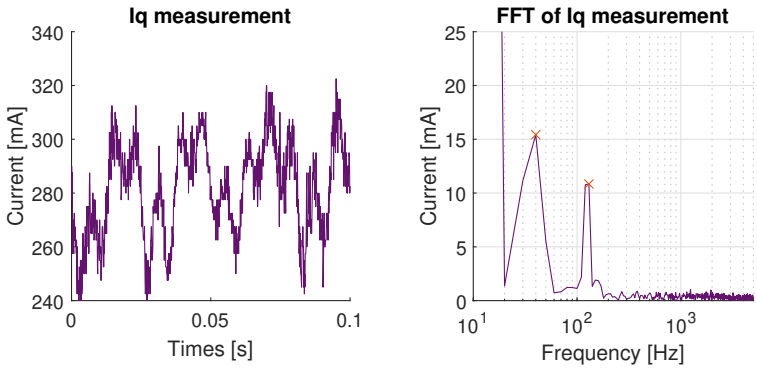

Figure 6.12: Measurement of the quadrature current at 64 Nmm reference torque, as well as the FFT of the same measurement.

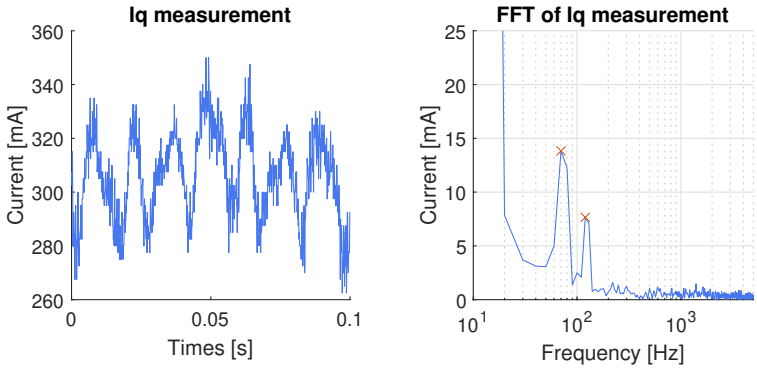

Figure 6.13: Measurement of the quadrature current at 70.4 Nmm reference torque, as well as the FFT of the same measurement.

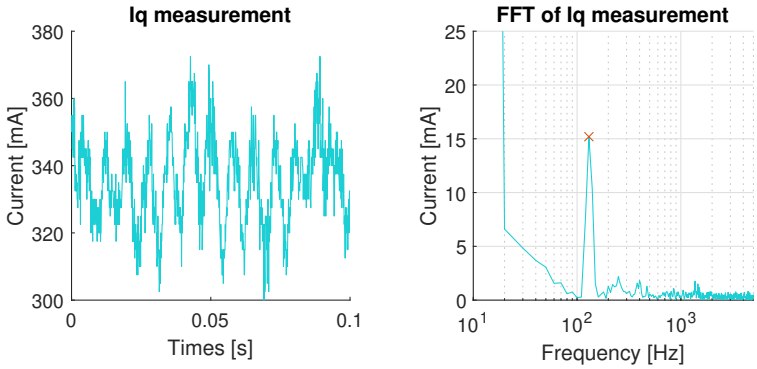

Figure 6.14: Measurement of the quadrature current at 76.8 Nmm reference torque, as well as the FFT of the same measurement.

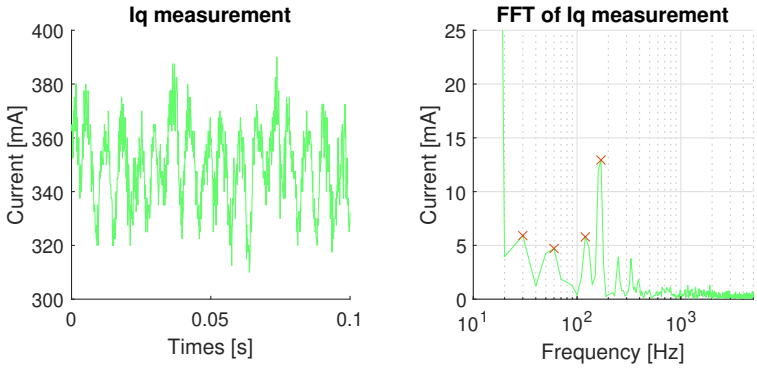

Figure 6.15: Measurement of the quadrature current at 80 Nmm reference torque, as well as the FFT of the same measurement.

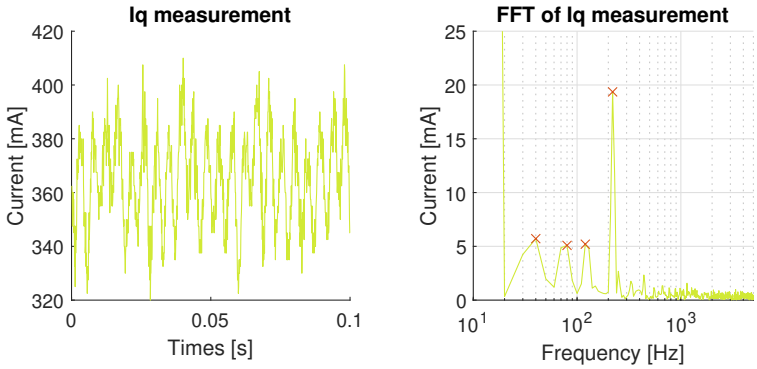

Figure 6.16: Measurement of the quadrature current at 83.2 Nmm reference torque, as well as the FFT of the same measurement.

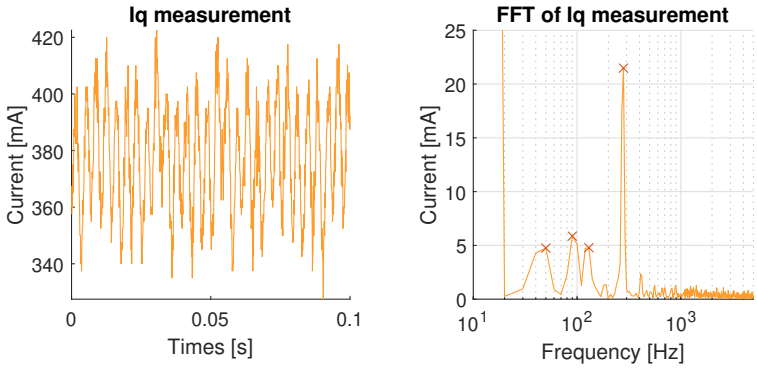

Figure 6.17: Measurement of the quadrature current at 86.4 Nmm reference torque, as well as the FFT of the same measurement.

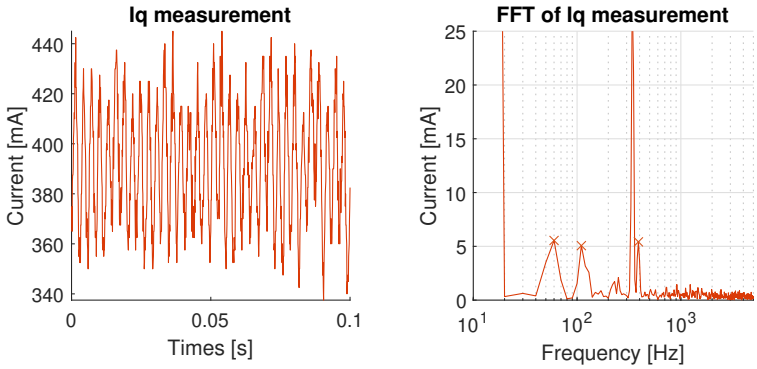

Figure 6.18: Measurement of the quadrature current at 89.6 Nmm reference torque, as well as the FFT of the same measurement.

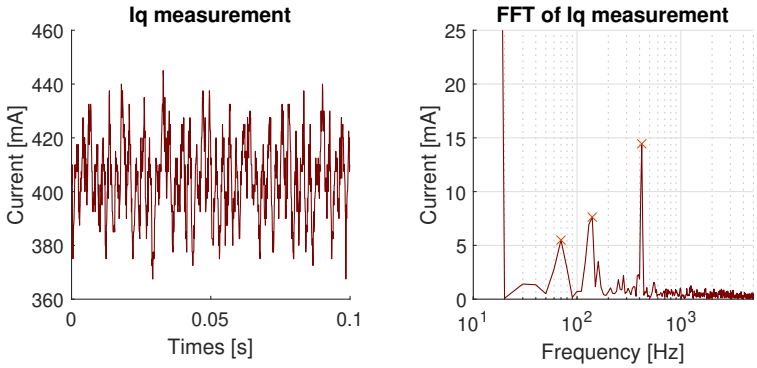

Figure 6.19: Measurement of the quadrature current at 92.8 Nmm reference torque, as well as the FFT of the same measurement.

Following the convention from the previous table, the manually added spikes are marked with asterisks in table 6.3. The electrical rotation speed is calculated as $w_e = w_m \cdot pp$, where pp is the number of pole pairs, which is equal to 4 in this case.

Table 6.4: Overview of the results regarding spectral analysis of the quadrature current.

	64 Nmm reference	**70.4 Nmm reference**	**76.8 Nmm reference**	**80 Nmm reference**	**83.2 Nmm reference**	**86.4 Nmm reference**	**89.6 Nmm reference**	**92.8 Nmm reference**
Electrical Rotation [Hz]	4.97	10.09	18.20	22.32	29.37	36.95	45.87	55.95
DC Component [mA]	284.8	314.2	337.1	350.0	365.2	377.6	392.3	404.8
Spike 1 [Hz]	40	70	130	30	40	50	60	70
Spike 2 [Hz]	130	120	N/A	120	80	90	110	140
Spike 3 [Hz]	N/A	N/A	N/A	170	120	130	340	420
Spike 4 [Hz]	N/A	N/A	N/A	250 *	220	280	390	N/A
Spike 5 [Hz]	N/A	N/A	N/A	330 *	N/A	410 *	N/A	N/A

Looking at the overview it can be seen that the resolution is quite poor at 10 Hz. This is caused by the software used to record the current measurement, which is limited to 1000 samples, which at the sampling frequency results in the FFT bins of 10 Hz [23]. A possible common spike between 120 and 130 Hz, with references 89.6 Nmm and 92.8 Nmm being the outliers showing a spike at 110 and 140 Hz, respectively. In an effort to clarify the relationship between these spikes the spectra are re-plotted together in figure 6.20.

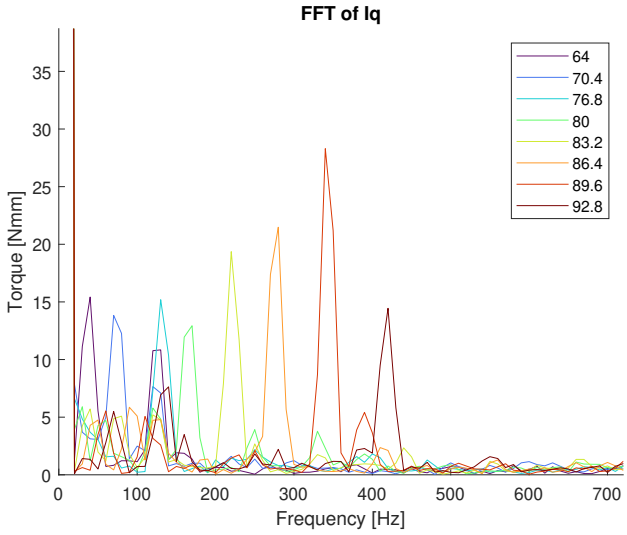

Figure 6.20: FFT of the I_q current of all quasistatic measurements. References are given in Nmm.

Viewing the data like this a common spike seems to be present around 125 Hz. It can be seen that although the peaks of the spikes do not line up perfectly at 125 Hz, they are all wide enough to overlap at this frequency.

In figure 6.21 the FFT of the same data can be seen, but with the x-axis rescaled to use per rev-

olution instead of frequency per second. This is done similarly to the spectra in 6.12-6.19.

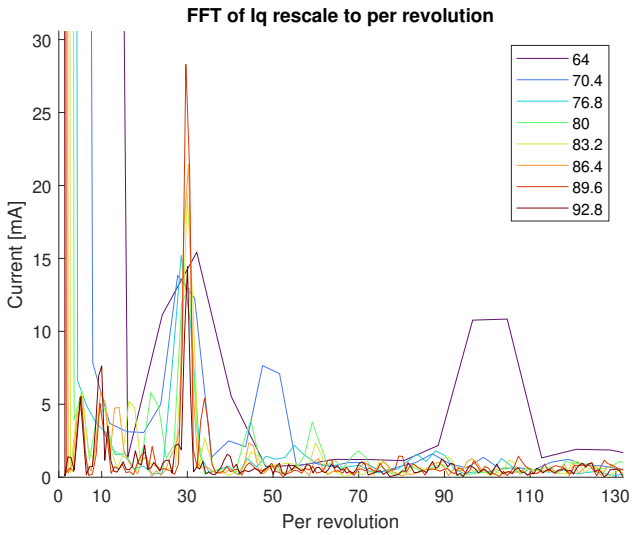

Figure 6.21: FFT of the I_q current of all quasi static measurements. References are given in Nmm.

When viewing the data like this a cluster of spikes can be observed around thirty times per revolution. This spike is present for all reference torques.

6.2 Static Tests

This section presents the results of the static tests. The positions tested are presented here as "P" followed by a number between 0 and 9. The number represents multiples of 10°, e.g. 0 represents 0 degrees and 1 represents 10 degrees. These degrees refer to mechanical position, which relates to the electrical as $\theta_m = \theta_e/4$. This means that one whole electrical rotation is completed in the tests. In table 6.5 an overview of the static measurements can be seen.

Table 6.5: An overview of the measurement results of the static test, as well as the calculated ideal torque, given the measured i_q values.

	T_{meas} $[Nmm]$	T_{calc} $[Nmm]$	i_q $[mA]$	i_d $[mA]$
64 Nmm Reference	61.1 ± 11.4	64.1 ± 9.7	280.1 ± 42.50	-0.04 ± 27.5
96 Nmm Reference	102.1 ± 17.3	96.1 ± 8.9	420.0 ± 38.75	0.04 ± 23.75
128 Nmm Reference	127.4 ± 9.2	128.7 ± 6.6	562.5 ± 28.75	0.02 ± 30.00
160 Nmm Reference	169.1 ± 16.2	160.7 ± 6.6	702.6 ± 28.75	0.11 ± 32.5
192 Nmm Reference	198.9 ± 9.3	193.3 ± 6.3	845.0 ± 27.50	-0.02 ± 32.5
224 Nmm Reference	242.8 ± 15.2	225.4 ± 5.1	985.3 ± 22.50	-0.01 ± 27.5
256 Nmm Reference	275.7 ± 9.6	258.0 ± 5.4	1127.7 ± 23.75	0.01 ± 28.75
288 Nmm Reference	313.3 ± 10.3	290.0 ± 6.0	1267.5 ± 26.25	0.04 ± 26.5
320 Nmm Reference	347.8 ± 11.4	322.6 ± 6.3	1410.0 ± 27.50	0.00 ± 27.5

Torque Measurements

Figures 6.22 - 6.30 show how the torque output varies with the position of the rotor, each figure shows one particular reference torque in all measured positions.

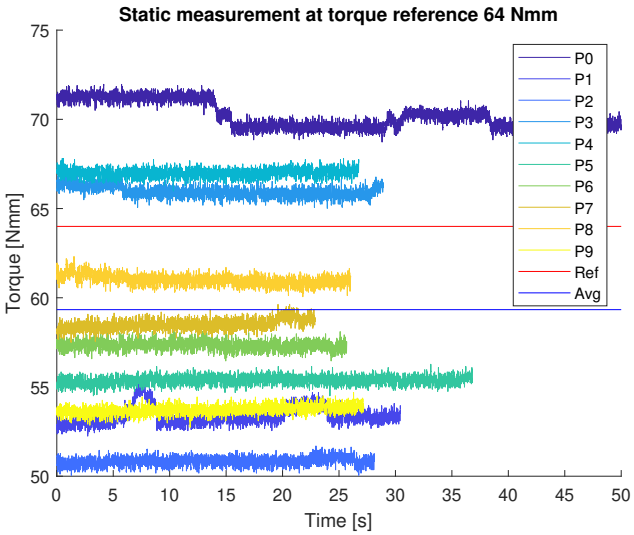

Figure 6.22: Torque output from the motor with a reference torque of 64 Nmm.

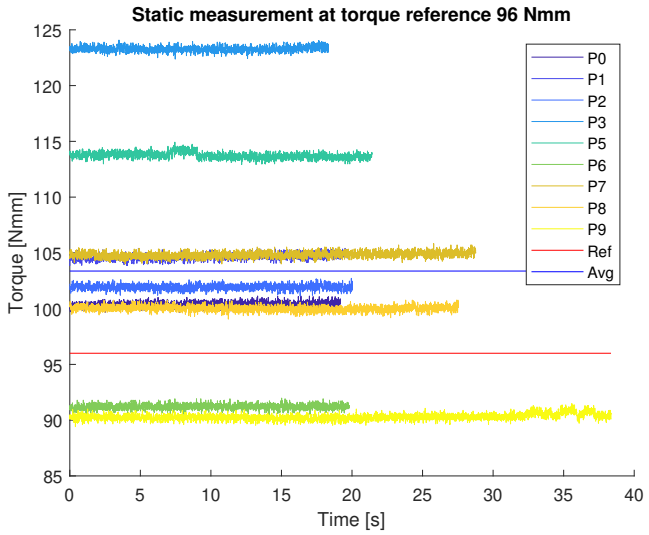

Figure 6.23: Torque output from the motor with a reference torque of 96 Nmm.

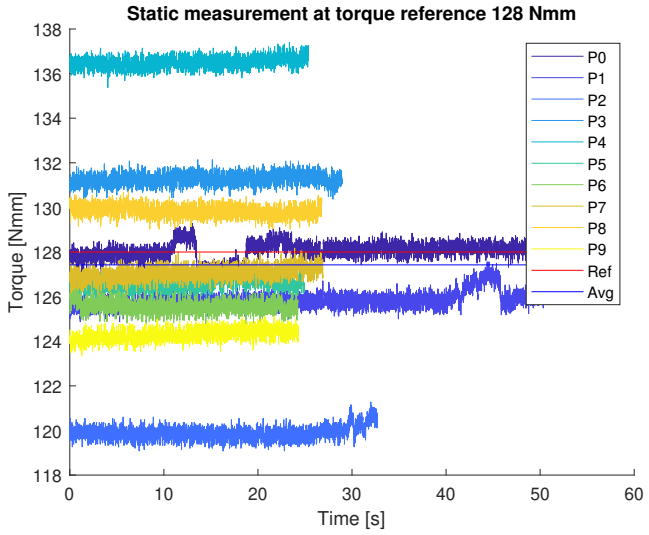

Figure 6.24: Torque output from the motor with a reference torque of 128 Nmm.

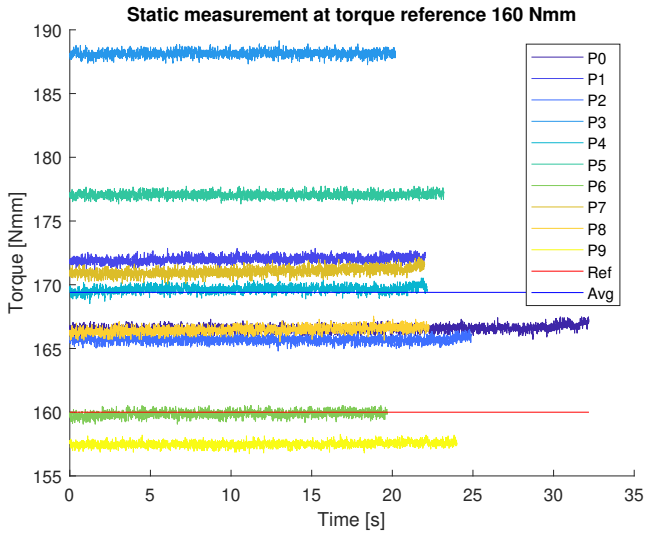

Figure 6.25: Torque output from the motor with a reference torque of 160 Nmm.

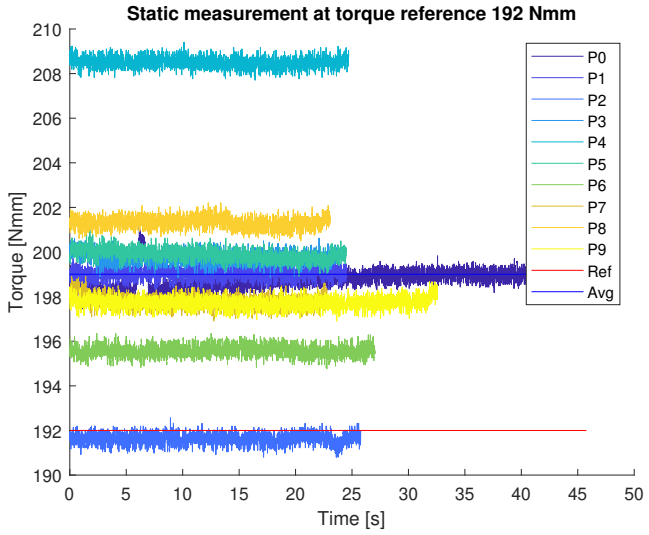

Figure 6.26: Torque output from the motor with a reference torque of 192 Nmm.

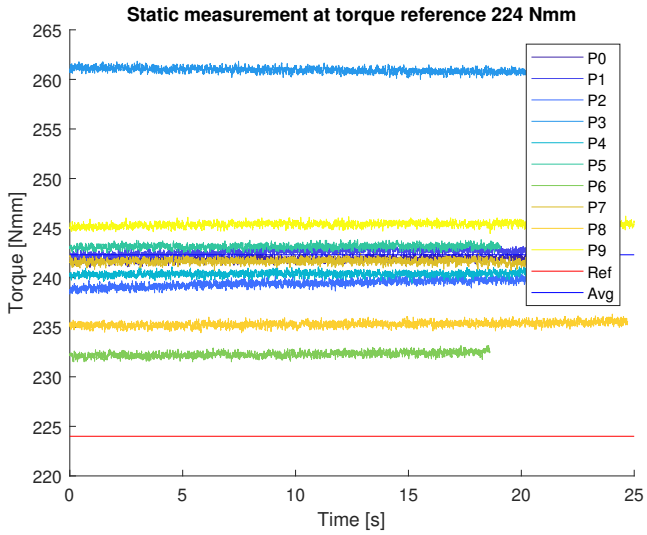

Figure 6.27: Torque output from the motor with a reference torque of 224 Nmm.

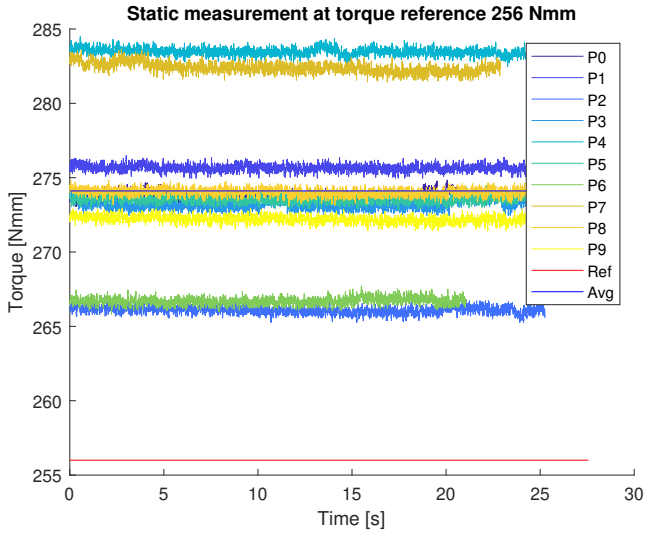

Figure 6.28: Torque output from the motor with a reference torque of 256 Nmm.

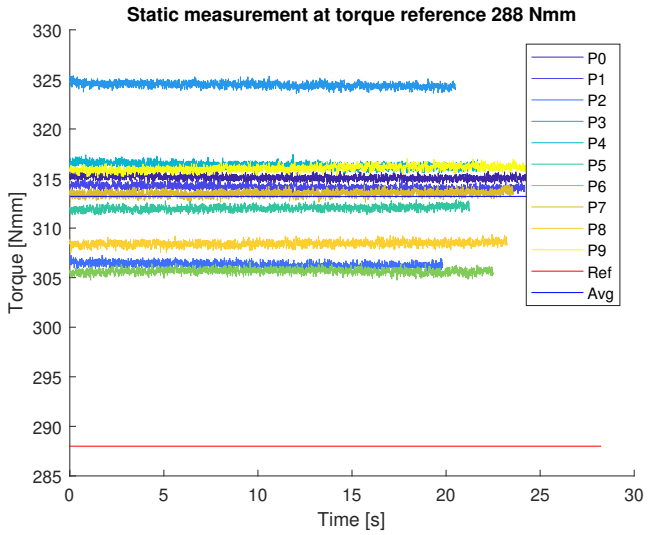

Figure 6.29: Torque output from the motor with a reference torque of 288 Nmm.

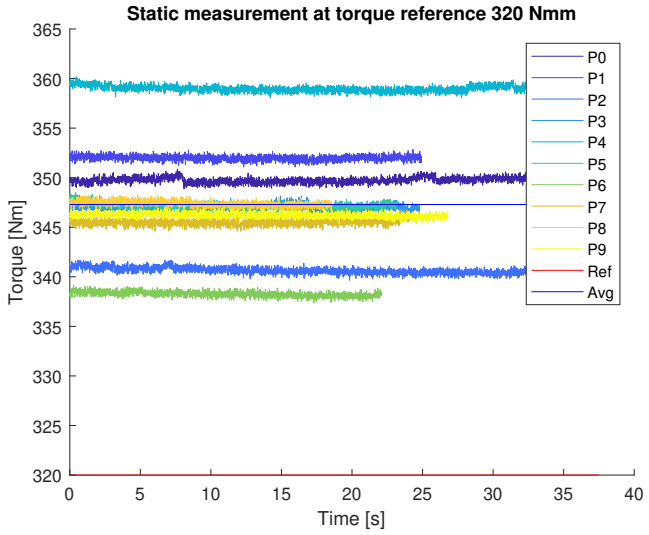

Figure 6.30: Torque output from the motor with a reference torque of 320 Nmm.

In an effort to make any potential relationship between torque variations and the position of the rotor visually discernible, the torque is plotted as a function of the position in figure 6.31. This figure, in conjunction with 6.32 also serves to show that the position is not varying significantly during measurements.

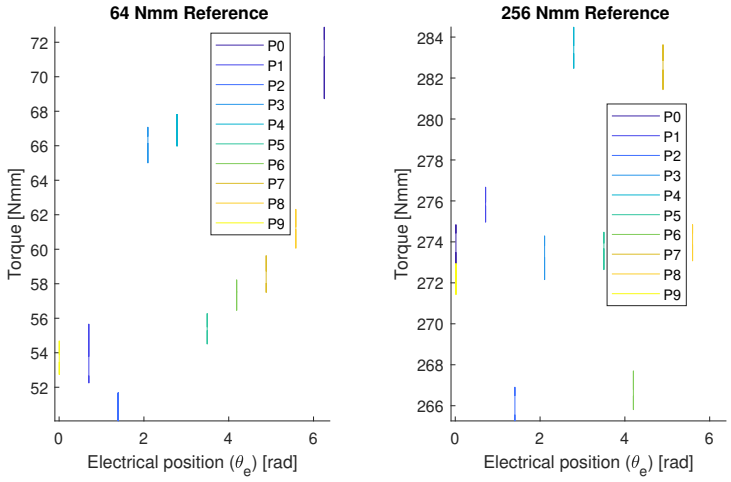

Figure 6.31: Measure torque compared to measure electrical position.

The torque is also plotted over 60 electrical degrees, as this matches the period of the saturation curve in figure 5.17.

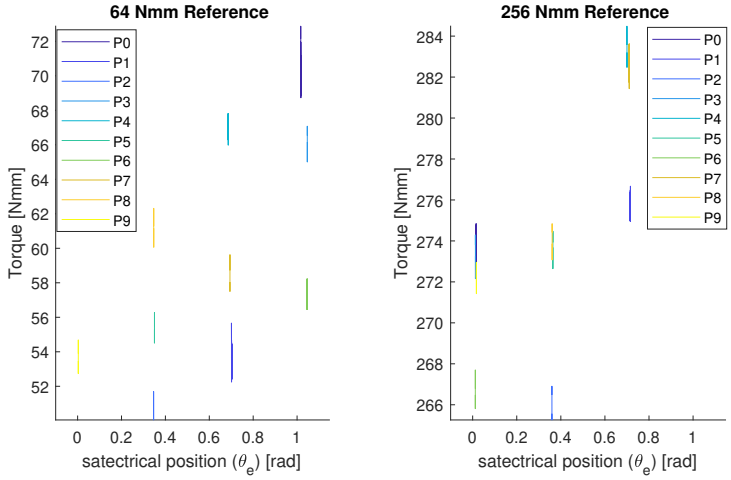

Figure 6.32: Measure torque compared to measure electrical position, but with a period of 1/4 of a revolution.

Current Measurements

Figure 6.33 is included to show some examples of the current measurements obtain in the static tests. No signs of positional dependency in the currents can be seen. The rest of the measurements are not shown since no interesting information can be obtained from the data.

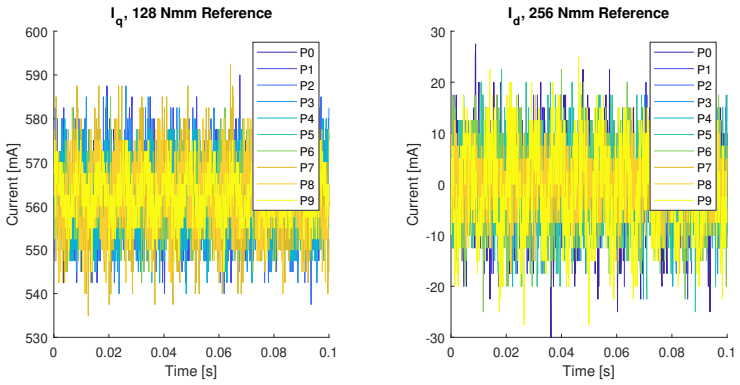

Figure 6.33: Raw data of electrical measurements from static tests.

To check for any common frequency components in the i_q currents the FFTs of the current measurements are shown in figure 6.34. All static measurements are presented together, and both the x- and y-axis are drawn using the logarithmic scale. Looking at the FFT of the static i_q measurements, a similar spike to that in the quasi static measurement can be seen at 130 Hz here too.

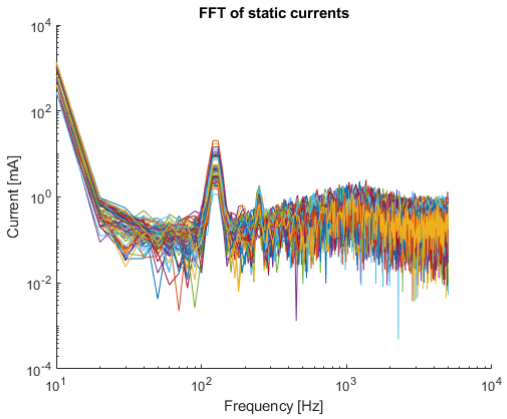

Figure 6.34: The FFTs of all static current measurements.

7 Discussion

This chapter aims to analyse the results of the thesis, explaining what they mean in this context, why (or why not) they are relevant, what can be ruled out and what could be improved or expanded upon.

7.1 Modelling

Drive System

Looking at the modelling in the ideal case we see the effects of the switching clearly, figures 5.2-5.4, which we were not able to see in the measured results. Since the information is lost as the switching is typically occurring at frequencies around 5-50 kHz, while the sampling in TwinCAT is done with a frequency of 4 kHz giving a Nyquist frequency of only 2 kHz [24]. The switching frequency of the drive unit is not known in this case, making it harder to spot any signs of its effects, the simulation however was run with a switching frequency of 25 kHz and is not sampled. However, seeing the switching frequency show up so clearly in the torque (figure 5.2) is unlikely to happen in practice because of the natural low pass filter properties of a mechanical system. This, in combination with no sign of a common high frequency signal being aliased to a lowered frequency in the FFT of the torque signals, suggests that this is a property of the simulation, not present in the torque of the real system. In the case of the current measurements, the sampling frequency is 10 kHz, equating to a Nyquist frequency of 5 kHz. While there is a chance for the switching frequency to be seen for these measurements, if it is low enough but as no spike is seen at 5 kHz this can be ruled out. As previously mentioned, the only common frequency spike in the current measurements is seen at 130 Hz, which if caused by aliasing, corresponds to a frequency of 29.87 kHz, or similarly illogical frequency. This once again points towards it not being cause by the switching behaviour of the driver.

When adding a disturbance to the system, a sinusoidal effect can be seen on the torque, as expected. It does however appear as larger in variation than the magnitude of the disturbance added. Looking at the simulated torque output in figure 5.5 the variation is about ± 14 Nmm, while the added disturbance only had an amplitude of 10 Nmm. This might be a property of the unsophisticated method used to introduce the disturbance, or it could be a property of the simulation. Looking at the simulated rpm, the rotation seems to be slowing down. This is assumed to be caused by the short simulation time (0.05 s) not allowing the system to reach its steady state. It should be noted however that the y-axis showing the rpm is chosen to show the variations in speed from the disturbance and is quite zoomed in. The largest and smallest rpm values shown only differ by about one rpm, including the contribution from the disturbance, and is therefore not seen as significant to the analysis. Comparing the currents seen in figure 5.6 to those seen in figure 5.3 we can see that the currents have not been affected. This is to be expected as no corrective measure of the current has yet been applied.

For the compensated torque seen in figure 5.7 a significant improvement can be seen when compared to figure 5.5, in both torque and rpm. It is however not perfectly compensated. One part of this is the switching of the signal, seen at this scale as the thickness of the torque line, for which compensation was not attempted. However, even when taking the switching into account, the disturbance does not seem to be perfectly compensated. The reason for this is assumed to be the fact that the size of the variation is larger than the introduced sinusoidal's amplitude, as the compensation is based on the latter. While some tweaking could probably rectify this, it was deemed as less important, as the interest was mainly in showing the possibility of compensation through this method and the real world issues are not well enough documented yet to make a

definitive choice of compensation method. Looking at the currents in figure 5.8 we can see the effects of the compensation current added to the system. The variation seen in the i_q current is a direct result of this and expected. The change in i_d current however is caused by the fact that these currents are just representations of reality to simply control and are in reality both combinations of the phase currents and therefore intertwined.

In figure 5.9 we see a completely different effect on the torque. In this case, the phase of the compensation is chosen with the opposite intention as before, to create the worst case scenario for this compensation method in the tested model. It should be noted that no difference can be seen when comparing the currents in figures 5.8 and 5.10, making the risk greater. A torque sensor is an expensive measuring device and not usually used for feedback in the control of servo motors, meaning that the poor performance of the torque output would not be seen by the controller. While this situation is fabricated, similar situations can occur in practice caused by e.g. changes to the motor properties due to age, making incorrect assumptions about the source of the issue etc.

FEM analysis

Looking at the two simulated magnetisations in figures 5.11-5.14 there are some slight differences is the magnetic flux density. The diametric magnetisation seems to have a slight lower flux, mainly seen by the slightly less orange rotor and not quite as bright orange colour in the stator. When comparing the torque production in relation to the current in figures 5.15-5.16 the DM rotor actually produces slightly higher torque compared to the radially magnetised rotor. This is opposite of what would be expected, as a higher magnetic flux should result in higher torque, all else being equal. This could be caused by magnetic saturation, but the effect was not investigated enough to say for certain in the context of this thesis. The variation in torque is fairly low, about one Nmm at zero current as seen in figure 5.16, implying that there should not be significant cogging in the machine. In figure 5.17, where the position of the rotor is taken into account, the RM produces the higher torque ripple in general and there does not seem to be any indication of significant ripple at zero ampere, again indicating low cogging.

Comparing figure 5.19 to 5.21 a pinkish area can be seen at about two o'clock in the latter figure, co-responding to the area where the gap is located, indicating a lower flux density when comparing to the yellows and reds seen in this area when no gap is present. In the figures showing loss density, 5.20 and 5.22, the iron losses appear fairly uniform throughout the stator yoke when no gap is present. Around the gap the in figure 5.22 the loss density is actually lower than in the same area without a gap. This might appear counterintuitive, but the reason for this is that the air gap is a poor magnetic conductor, causing the magnetic flux to choose another path with less magnetic reluctance, leading to less magnetic loss in the area. This leads to the increase in loss seen in the areas surrounding the gap as the flux takes this path instead, leading to higher losses in these areas. The effects of a potential stator gap on the torque output can be seen in figure 5.23. In the blue line showing the gap-less torque, a ripple occurring 18 times in an electric revolution can be seen. This is the same as 72 times in a mechanical revolution and matches the cogging frequency calculated through equation 2. This is not the source of the cogging torque, but an interesting coincidence nonetheless. The ripple seems to have a magnitude of about ± 5 Nmm. There is also an offset of about 24 Nmm, the source of which is the magnetic hysteresis taking place in the stator. Adding a gap creates a larger torque ripple with a frequency of two times per electrical revolution, eight times per mechanical. Looking carefully at the waveform, the ripple seen without a gap also seems to be present within the torque ripple for the simulated gap. This is most evident when looking at the overlap of the two graphs. Figure 5.24 shows how

the irons losses are related to electrical angle with and without a stator gap. With no gap the loss is fairly uniform over an electrical revolution, when adding a gap two large spikes can be seen occurring twitch per revolution.

7.2 Measurements

In the initial phases of this thesis work, it was assumed that the issues of variations in the output torque originated from cogging in the motor. This assumption was attained from information given by the manufacturer. The preliminary FEM work however did not support this hypothesis and neither do the results from the measurements. This also means that the methods formulated to test the torque were design to find a connection between the ripple and the position of the rotor.

Quasi static measurements

Looking at the overview in table 6.1 the calculated ideal torque, T_{calc}, based on the i_q measurements actually fluctuates more than the measured torque, in all but one case. This would lead one to believe that a poor following of the reference is enough to explain the variations in torque output. It should be noted though that the electrical measurements only represent a very short time span of 0.1 s, because of limitations in the software. There also seems to be a correlation between the physical angle of the rotor and the torque variations, as seen by the spikes matching a discrete number of occurrences per revolution in figures 6.4-6.11 and table 6.2. These do not however line up with the expected frequency of cogging in the machine. The first few multiples of the base rotations speeds two, four and eight, seem to line up with common mechanical issues in motors, such as axial misalignment, bearing defects or the couplers effect on the system [15]. The last spike that is seen in multiple measurements is seen 24 times per revolution. This matches the period of torque ripple caused by magnetic saturation shown in figure 5.24, as the electrical period is completed four times per mechanical, and the saturation period is completed 6 times per electrical period. Another possible source for this behaviour is the phenomenon described in 2.4, under the subchapter *Inverter Dead Time*.

From the electrical measurements, spikes with a decent match to 130 Hz (figure 6.20) can be seen for all measurements. When compensating for the speed of the rotation another common spike can be observed, occurring thirty times per mechanical revolution (fig. 6.21). These observations do not match up with the ones made from the torque measurements. There are significant limitations in the current measurements done, as it is only possible to log 1000 samples per measurement in the software. This means that while the torque measurements spans a time of around 40 seconds, the current measurements only span 0.1 seconds, making them less reliable. The low number of samples also greatly limits the resolution in the frequency domain, to 10 Hz.

Static measurements

Looking at the static measurements, the variations seen are larger than those seen in the static measurements, compare T_{meas} in table 6.1 to it in 6.5. This variation does not seem to be linked to the position of the rotor, however. For instance, "P5" (turquoise)in figure 6.22 has a lower value than both the reference and the average, while the same position in figure 6.23 is higher than both.

Looking at figures 6.31 and 6.32 no link can be found between the electrical period, nor 1/4 of the electrical period (as derived from the magnetic saturation) and the torque either. These figures also show that no significant drift in position during the measurements is present. No

answer can be gained from the current measurements either, as seen in figure 6.33, the i_q and i_d currents do not vary significantly between different positions.

Other sources that were discussed include temperature and friction. As a motor is running, it heats up, causing changes in the electrical properties of the motor, as well as in friction and thermal expansion. This is not seen as a likely cause since each test is less than a minute long and the motor is not being pushed particularly hard in the majority of tests. The clear difference in torque measurement between tests and the lack of drifting within each test also goes against temperature as a source. In addition, the temperature would have an impact on the quasi static tests as well. In the case of friction, the static or limiting friction would affect the static results far more than the quasi static, giving some reasoning to the strange behaviour of the torque in the static tests [25].

7.3 Improvements

Here some possible point of improvements will be presented. A lot of experience was gained in this process as it was not very typical work for Cognibotics. This naturally means that points of improvements arouse during the process, some which were possible to act upon immediately and others which could not be implemented at the time for one reason or another.

Modelling

For the modelling, some parameters are not well known, such as the rotor inertia and the switching frequency. In addition, due to the human factor, the incorrect values for the inductances of the motor were used, compare values in 4.2 with those listed in chapter 5.1. By evaluating these and finding more reliable values, a more trusted model could be set up. From there, different sources of disturbances could be modelled, to find a suitable match with the measured results.

Test bench improvements

With limited time and access to material and tools, there are a few points of improvements possible for the measurement bench made for and used in this thesis work. As the base was reused from old lab equipment, the possible precision was limited and could definitely be improved upon. The inertia wheel as well as its fastening and bearings were also reused and not rigorously tested. To fasten the motor and torque transducer to the baseplate, some pieces were 3d-printed in PLA plastic. These pieces are not very rigid and should be replaced with a more rigid material for a more reliable result. The axial alignment of the test bench also leaves room for improvement. Attempts were made to verify the alignment using dial indicators, similarly to what can be seen in [26]. However, limited time as well as the small physical size of the parts involved made this too cumbersome.

Measurements

As of now the current measurements used are not independently acquired, instead the manufacturer's built in hardware solutions were used. These should be properly validated if they are to be relied upon, as it is their product's performance that is being evaluated. Having access to direct measurements of the phase currents would also be a good addition to the measurements taken here. In addition to the hardware limitations, the software used to log the current was severely limited, only allowing 1000 samples to be logged, with time intervals of multiples of 100 microseconds (100 μs, 200 μs, 300 μs, etc.). Some features were not accessible from the start as they needed administrator access, which was not obtained until later into the thesis work. Mainly

the ability to log the position in the manufacturer's software would have been helpful as to make connecting the exact current values of a sample to its torque value, logged in TwinCAT.

In addition to this the official proprietary cabling for the torque transducer was not available making access to the data inconvenient. This coupled with poor documentation of the actually signal being sent left some decisions up to engineering intuition, which while offering quite good learning opportunities do not make for the most reliable academic results.

8 Conclusion and Future Work

In the last chapter of this thesis, a summary of what is done and what is shown from this is presented.

8.1 What was done

This thesis was done with the goal of identifying and compensating torque ripple effects in a 200 W permanent magnet synchronous servo motor, being used in robot applications. The machine design uses 8 poles and 9 teeth. An experimental setup is built to analyse the ripple. This is done in conjunction with machine and drive system evaluation models to build a better understanding of the causes of torque ripple. Two methodologies are used when performing the tests, referred to as quasi static and static. In the quasi static tests, the torque reference of the controller is unchanged during the test and the motor can rotate freely. In the static test, the torque reference is still unchanged during the test, but now the motor axis is fixed in place. The purpose of the quasi-static test is to study the pulsation spectrum of the torque, while static tests show the change of torque under load in several rotor positions.

8.2 What was concluded

The previously suspected cause, cogging torque, which is inherent to the motor and present at zero load, is shown not to be the cause. The ripple is shown to be linked to the sixth electric harmonic. Some lower harmonics are also present throughout the testing, but are likely introduced by the test setup. The origin of the pulsation is distinguished between mechanical (shaft and related components), electromagnetic (electrical machine) and drive system (power electronic control and feedback). From the experiments and analysis of the electrical machine, it can be concluded that the sixth electrical harmonic is caused by magnetic saturation and core loss. To reduce the impact on the torque of these effects, harmonic current injection is purposed.

8.3 Future Work

During the whole thesis work, the motor and driver were always run together as a unit, making it hard to distinguish which was the culprit of the issues. Testing these individually to evaluate their performance when match with other equipment of good behaviour (or at least well documented) would be of great interest. Another possibility is to do a separate, more detailed evaluations of the behaviour of the driver. One point of interest being looking into how the inverter dead time is being handled, as it is a likely candidate for the ripple.

Better knowledge of when the issues actually appears in practice could also greatly help in diagnosing the issues. This thesis was structured with the initial impression that the source was known to be the cogging torque, affecting the planning structure and how the tests were set up. Looking closer at the mentioned sources for the different disturbances and formulating a test methodology for these effects specifically should be done to evaluate them properly.

References

[1] Adhavan Balashanmugham and Mockaisamy Maheswaran. Permanent-magnet synchronous machine drives. In Adel El-Shahat and Mircea Ruba, editors, *Applied Electromechanical Devices and Machines for Electric Mobility Solutions*, chapter 2. IntechOpen, Rijeka, 2020.

[2] Tore Hägglund. *Reglerteknik AK Föreläsningar*. Institutionen för Reglerteknik LTH, Box 118 221 00 Lund, 2007.

[3] Song Wang. Adrc and feedforward hybrid control system of pmsm. *Mathematical Problems in Engineering*, 2013:1–12, 12 2013.

[4] S. Haddadin L. Johannsmeier, M. Gerchow. A robot manipulation framework: Learning the peg-in-hole task. `https://www.youtube.com/watch?v=ojpJlXIiTYE`.

[5] G. Dajaku and D. Gerling. New methods for reducing the cogging torque and torque ripples of pmsm. In *2014 4th International Electric Drives Production Conference (EDPC)*, pages 1–7, 2014.

[6] C. Studer, A. Keyhani, T. Sebastian, and S. K. Murthy. Study of cogging torque in permanent magnet machines. In *IAS '97. Conference Record of the 1997 IEEE Industry Applications Conference Thirty-Second IAS Annual Meeting*, volume 1, pages 42–49 vol.1, 1997.

[7] L. Dosiek and P. Pillay. Cogging torque reduction in permanent magnet machines. *IEEE Transactions on Industry Applications*, 43(6):1565–1571, 2007.

[8] L. Gasparin, A. Cernigoj, S. Markic, and R. Fiser. Additional cogging torque components in permanent-magnet motors due to manufacturing imperfections. *IEEE Transactions on Magnetics*, 45(3):1210–1213, 2009.

[9] Vinicius LOPES SIMOES, Najla HAJE OBEID, Fabien VIDAL NAQUET, and Gianluca ZITO. Permanent magnet synchronous motor current harmonic compensation method using model predictive control. In *2020 IEEE 29th International Symposium on Industrial Electronics (ISIE)*, pages 179–184, 2020.

[10] C. J. O'Rourke, M. M. Qasim, M. R. Overlin, and J. L. Kirtley. A geometric interpretation of reference frames and transformations: dq0, clarke, and park. *IEEE Transactions on Energy Conversion*, 34(4):2070–2083, 2019.

[11] Per Karlsson Mats Alaküla. *Power Electronics Devices, Converters, Control and Applications*. Lund University Department of Electrical Engineering and Automation, 2015.

[12] Dara O'Sullivan Jens Sorensen. A system approach to understanding the impact of nonideal effects in a motor drive current loop. *Analog Devices, Inc.*, 2016.

[13] S. Kaitwanidvilai, W. Khan-Ngern, and M. Panarut. The impact of deadtime effect on unwanted harmonics conducted emission of pwm inverters. In *Proceedings. Asia-Pacific Conference on Environmental Electromagnetics. CEEM'2000 (IEEE Cat. No.00EX402)*, pages 232–237, 2000.

[14] Qinpeng Huang, Weikun Niu, Haiping Xu, Cheng Fang, and Lei Shi. Analysis on dead-time compensation method for direct-drive pmsm servo system. In *2013 International Conference on Electrical Machines and Systems (ICEMS)*, pages 1271–1276, 2013.

[15] Jason Mais. Spectrum analysis the key features of analyzing spectra. `https://www.skf.`

com/binaries/pub12/Images/0901d1968024acef-CM5118-EN-Spectrum-Analysis_tcm_12-113997.pdf.

[16] T. M. Jahns and W. L. Soong. Pulsating torque minimization techniques for permanent magnet ac motor drives-a review. *IEEE Transactions on Industrial Electronics*, 43(2):321–330, 1996.

[17] R. Islam, I. Husain, A. Fardoun, and K. McLaughlin. Permanent magnet synchronous motor magnet designs with skewing for torque ripple and cogging torque reduction. In *2007 IEEE Industry Applications Annual Meeting*, pages 1552–1559, 2007.

[18] G. Ferretti, G. Magnani, and P. Rocco. Modeling, identification, and compensation of pulsating torque in permanent magnet ac motors. *IEEE Transactions on Industrial Electronics*, 45(6):912–920, 1998.

[19] G. Lee, S. Kim, J. Hong, and J. Bahn. Torque ripple reduction of interior permanent magnet synchronous motor using harmonic injected current. *IEEE Transactions on Magnetics*, 44(6):1582–1585, 2008.

[20] H. Jia, M. Cheng, W. Hua, W. Zhao, and W. Li. Torque ripple suppression in flux-switching pm motor by harmonic current injection based on voltage space-vector modulation. *IEEE Transactions on Magnetics*, 46(6):1527–1530, 2010.

[21] ComInTec. Elastomeric couplings - rigid couplings. https://www.bengtssons-maskin.se/uploads/extrafiles_file_172.pdf.

[22] Iea power electronics - components, converters, control and applications (eien 25). https://www.iea.lth.se/kel/.

[23] Michael Cerna and Audrey F. Harvey. The fundamentals of fft-based signal analysis and measurement. http://www.lumerink.com/courses/ece697/docs/Papers/The%20Fundamentals%20of%20FFT-Based%20Signal%20Analysis%20and%20Measurements.pdf.

[24] Karl-Erik Årzén. *Real-Time Control Systems*. Department of Automatic Control Lund University, 2014.

[25] Dorian Hanaor, Yixiang Gan, and Itai Einav. Static friction at fractal interfaces. *Tribology International*, 93:229–238, 01 2016.

[26] Cummins Generator Technologies. Agn 234 - generating set assembly - alignment. https://www.stamford-avk.com/sites/stamfordavk/files/AGN234_A.pdf.